Circulation

ORIGINAL RESEARCH ARTICLE

Human Hereditary Cardiomyopathy Shares a Genetic Substrate With Bicuspid Aortic Valve

Marcos Siguero-Álvarez, PhD; Alejandro Salguero-Jiménez, PhD; Joaquim Grego-Bessa, PhD; Jorge de la Barrera, MSc; Donal MacGrogan, PhD; Belén Prados, PhD; Fernando Sánchez-Sáez, MSc; Rebeca Piñeiro-Sabarís, MSc; Natalia Felipe-Medina, PhD; Carlos Torroja, PhD; Manuel José Gómez, PhD; María Sabater-Molina, PhD; Rubén Escribá, PhD; Ivonne Richaud-Patin, PhD; Olalla Iglesias-García, PhD; Mauro Sbroggio, PhD; Sergio Callejas, PhD; Declan P. O'Regan, MD, PhD; Kathryn A. McGurk, PhD; Ana Dopazo, PhD; Giovanna Giovinazzo, PhD; Borja Ibañez, MD, PhD; Lorenzo Monserrat, MD, PhD; José María Pérez-Pomares, PhD; Fátima Sánchez-Cabo, PhD; Alberto M. Pendas, PhD; Angel Raya, PhD; Juan R. Gimeno-Blanes, MD, PhD; José Luis de la Pompa, PhD

BACKGROUND: The complex genetics underlying human cardiac disease is evidenced by its heterogenous manifestation, multigenic basis, and sporadic occurrence. These features have hampered disease modeling and mechanistic understanding. Here, we show that 2 structural cardiac diseases, left ventricular noncompaction (LVNC) and bicuspid aortic valve, can be caused by a set of inherited heterozygous gene mutations affecting the NOTCH ligand regulator MIB1 (MINDBOMB1) and cosegregating genes.

METHODS: We used CRISPR-Cas9 gene editing to generate mice harboring a nonsense or a missense *MIB1* mutation that are both found in LVNC families. We also generated mice separately carrying these *MIB1* mutations plus 5 additional cosegregating variants in the *ASXL3*, *APCDD1*, *TMX3, CEP192*, and *BCL7A* genes identified in these LVNC families by whole exome sequencing. Histological, developmental, and functional analyses of these mouse models were carried out by echocardiography and cardiac magnetic resonance imaging, together with gene expression profiling by RNA sequencing of both selected engineered mouse models and human induced pluripotent stem cell–derived cardiomyocytes. Potential biochemical interactions were assayed in vitro by coimmunoprecipitation and Western blot.

RESULTS: Mice homozygous for the *MIB1* nonsense mutation did not survive, and the mutation caused LVNC only in heteroallelic combination with a conditional allele inactivated in the myocardium. The heterozygous *MIB1* missense allele leads to bicuspid aortic valve in a NOTCH-sensitized genetic background. These data suggest that development of LVNC is influenced by genetic modifiers present in affected families, whereas valve defects are highly sensitive to NOTCH haploinsufficiency. Whole exome sequencing of LVNC families revealed single-nucleotide gene variants of *ASXL3*, *APCDD1*, *TMX3, CEP192*, and *BCL7A* cosegregating with the *MIB1* mutations and LVNC. In experiments with mice harboring the orthologous variants on the corresponding *Mib1* backgrounds, triple heterozygous *Mib1 Apcdd1 Asxl3* mice showed LVNC, whereas quadruple heterozygous *Mib1 Cep192 Tmx3;Bcl7a* mice developed bicuspid aortic valve and other valve-associated defects. Biochemical analysis suggested interactions between CEP192, BCL7A, and NOTCH. Gene expression profiling of mutant mouse hearts and human induced pluripotent stem cell–derived cardiomyocytes revealed increased cardiomyocyte proliferation and defective morphological and metabolic maturation.

CONCLUSIONS: These findings reveal a shared genetic substrate underlying LVNC and bicuspid aortic valve in which MIB1-NOTCH variants plays a crucial role in heterozygous combination with cosegregating genetic modifiers.

Key Words: BAV ■ cardiomyopathy ■ genetic modifiers ■ LVNC ■ MIB1 ■ NOTCH ■ valves

Correspondence to: José Luis de la Pompa, PhD, Intercellular Signaling in Cardiovascular Development & Disease Laboratory, Centro Nacional de Investigaciones Cardiovasculares, Melchor Fernández Almagro 3, 28029 Madrid, Spain. Email jlpompa@cnic.es

Supplemental Material is available at https://www.ahajournals.org/doi/suppl/10.1161/CIRCULATIONAHA.121.058767.

For Sources of Funding and Disclosures, see page XXX.

Circulation is available at www.ahajournals.org/journal/circ

ORIGINAL RESEARCH ARTICLE

Clinical Perspective

What Is New?

- Heterozygous mutations in the NOTCH regulator *MIB1* lead to human left ventricular noncompaction (LVNC), but cause LVNC or bicuspid aortic valve (BAV) in a NOTCH-sensitized mouse genetic background.
- Whole exome sequencing of LVNC families has identified heterozygous missense mutations in 5 genes, cosegregating with MIB1 and LVNC. The corresponding mouse models show LVNC or BAV in a NOTCH-sensitized genetic background.
- Gene profiling shows increased cardiomyocyte proliferation and defective morphological and metabolic maturation in mouse hearts and human induced pluripotent stem cell–derived cardiomyocytes. Biochemistry suggests a direct interaction between NOTCH and some of the identified gene products.
- These data support a shared genetic basis for LVNC and BAV with MIB1-NOTCH playing a crucial role.

What Are the Clinical Implications?

- Novel insights into the genetic basis and oligogenic nature of LVNC.
- Identification of heterozygous mutations leading to LVNC (*MIB1 ASXL3 APCDD1*) or BAV (*MIB1 CEP192 TMX3; BCL7A*) may allow expansion of the genetic testing panel repertoire for better diagnosis and/or stratification of patients with LVNC and BAV.
- Whether patients with LVNC have a higher prevalence of BAV remains uncertain, and further evaluation is required.

Nonstandard Abbreviations and Acronyms

APCDD1	APC down-regulated 1
ASXL3	ASXL transcriptional regulator 3
BAV	bicuspid aortic valve
BCL7A	BAF chromatin remodeling complex subunit BCL7A
CEP192	centrosomal protein 192
co-IP	coimmunoprecipitation
CT	C-terminal fragment
E	embryonic day
EMT	EPITHELIAL_TO_MESENCHYMAL_TRANSITION
GATK	Genome Analysis Toolkit
GERP	genomic evolutionary rate profiling
hiPSC	human induced pluripotent stem cell
hiPSC-CM	human induced pluripotent stem cell–derived cardiomyocyte
iPSC	induced pluripotent stem cell
LVNC	left ventricular noncompaction
MIB1	MIB E3 ubiquitin protein ligase 1
N1ICD	NOTCH1 intracellular domain
NOTCH1	NOTCH receptor 1
PCR	polymerase chain reaction
RNA-seq	RNA sequencing
ssODN	single-stranded donor oligonucleotides
RBPJ	recombining binding protein suppressor of hairless
SNP	single nucleotide polymorphism
TMX3	thioredoxin related transmembrane protein 3
Tnnt2	cardiac troponin T
WB	Western blot
WES	whole exome sequencing

The genetic basis of cardiovascular disease is poorly understood, and it is only with the advent of new high-throughput DNA sequencing techniques that a picture has begun to emerge of its complexity and the difficulty of establishing direct genotype-phenotype correlations. Cardiomyopathies were initially thought to be monogenic disorders; however, phenotypic expressivity and penetrance have been found to be affected by variable presentation within a family with the same mutation,[1] the influence of multiple genetic variants and their epistatic relationships, and epigenetic and environmental factors.[2,3]

Left ventricular noncompaction (LVNC) is the third most common cardiomyopathy (prevalence, 0.05%[4]) and is characterized by the presence of excessive trabeculae with deep recesses in the left ventricle.[5,6] Trabeculae are endocardial cell–covered cardiomyocyte bundles in the vertebrate ventricle that facilitate oxygen and nutrient exchange.[7] As development proceeds, the outer compact myocardium layer expands by proliferation, contributing to the integration of trabeculae in the ventricular wall through the poorly understood process of compaction,[8,9] which coincides with the invasion of the myocardium by the coronary vasculature.[8,10] Familial LVNC has been attributed to defective ventricular maturation and compaction in utero[5,11] and is characterized by a dilated left ventricle and associated systolic dysfunction.[5] In addition, zones of fibrotic tissue related to disease severity might be dispersed on the endocardial surfaces.[12] One of the echocardiographic diagnosis criteria for LVNC is a ratio of noncompacted to compacted myocardium of ≥2 at end-systole.[13,14] Clinical presentation of LVNC ranges from asymptomatic cases to severe heart failure requiring heart transplantation.[15–17]

LVNC is genetically heterogeneous, with a predominantly autosomal-dominant inheritance pattern,[18] and has been linked to sarcomere gene mutations, particularly in *MYH7*.[19,20] Other mutations implicated in LVNC affect genes encoding the scaffold protein α-dystrobrevin and

the nuclear protein lamin A/C.[21,22] The proposed developmental origin of LVNC has prompted suggestions of the involvement of genetic alterations of the signals and transcription factors that regulate cardiovascular development.[23–25] A key mediator of cell fate specification and tissue patterning in metazoans is the highly conserved signaling pathway NOTCH,[26,27] and NOTCH signaling disruption in humans leads to developmental abnormalities affecting the heart and vessels.[28–31] Studies in targeted mutant mice have shown that NOTCH is crucial for the endocardium-to-myocardium signaling processes that govern cardiac valve and ventricle development and have shed light on the disease mechanisms associated with NOTCH dysfunction (see reviews[32,33]). We showed that LVNC in mice and humans can be caused by mutations in the ubiquitin ligase MIB1 (MINDBOMB1),[34] which is required for NOTCH ligand endocytosis and signaling activation.[35]

Here, we used CRISPR-Cas9 gene editing and whole exome sequencing (WES) to study LVNC inheritance in 2 large families carrying *MIB1*-inactivating mutations.[34] The Mib1^{R530X} nonsense mutation causes LVNC in mice in heteroallelic combination with a conditional Mib1^{flox} allele, whereas the Mib1^{V943F} missense allele leads to bicuspid aortic valve (BAV) in a NOTCH-sensitized genetic background. We identified single-nucleotide variants in the *ASXL3*, *APCDD1*, *TMX3, CEP192*, and *BCL7A* genes that cosegregate with the *MIB1* mutations and LVNC in our pedigrees. Triple heterozygous *Mib1 Apcdd1 Asxl3* mutant mice develop features of LVNC, whereas quadruple heterozygous *Mib1 Cep192 Tmx3;Bcl7a* mice develop BAV and valve-associated defects. Coimmunoprecipitation (co-IP) analysis confirmed interaction among CEP192 (centrosomal protein 192), BCL7A (BAF chromatin remodeling complex subunit BCL7A), and NOTCH protein products. Gene profiling of mouse hearts and human induced pluripotent stem cell (hiPSC)–derived cardiomyocytes (hiPSC-CM) revealed a common defect in metabolism and cardiomyocyte maturation. These findings provide evidence for a shared genetic substrate underlying LVNC and BAV composed of MIB1-NOTCH and a set of genetic modifiers.

METHODS

Data Availability

The authors declare that all data that support the findings of this study are available within the article and its Supplemental Material. The data, analytical methods, and study materials will be available to other researchers for purposes of reproducing the results or replicating the procedure. The RNA sequencing (RNA-seq) data are deposited in the NCBI GEO database under accession number GSE185395. The UK Biobank data in this article are available from http://www.ukbiobank.ac.uk/.

Ethics and DNA collection

Clinical evaluations and genetic studies were performed in accordance with the principles of the Helsinki Declaration, and after informed consent of participating subjects for inclusion according to the protocol approved by the Ethics Committee of Clinical Research from the Hospital Universitario Virgen de la Arrixaca (218/C/2020). All patients underwent a clinical evaluation, including an ECG and 2-dimensional and Doppler echocardiography. A pedigree was drawn for each patient, and first-degree relatives were screened with the same protocol. Blood samples were taken for genetic analysis, and all patients and their relatives gave written informed consent. Genomic DNA was obtained from 1-mL blood samples extracted in EDTA using the DNAEasy Blood & Tissue Kit (Qiagen, 69506).

Mice

Established mouse strains used in this study were Tnnt2^{Cre} (Tnnt2: cardiac troponin T),[36] Myh6^{Cre},[37] Nkx2.5^{Cre},[38] Mib1^{flox},[39] and Notch1^{KO}.[40] The following new mouse lines were generated as part of this study: Mib1R530X/+, Mib1V943F/+, Mib1R530X/+ Asxl3M1361V/+ Apcdd1V150I/+, Mib1V943F/+ Cep192T1522M/+ Tmx3$^{F191X/+}$, Bcl7a$^{AG,GA/+}$, R26MIB1$^{V943F/+}$, and R26MIB1$^{WT/+}$ (see "Generation of New Mouse Lines"). Genotyping details will be provided on request.

Animal studies were approved by the Centro Nacional de Investigaciones Cardiovasculares Animal Experimentation Ethics Committee and by the Community of Madrid (Ref. PROEX 155.7/20). All animal procedures conformed to EU Directive 2010/63EU and Recommendation 2007/526/EC on the protection of animals used for experimental and other scientific purposes, enacted in Spanish law under Real Decreto 1201/2005.

Generation of New Mouse Lines

To generate the Mib1$^{R530X/+}$ and Mib1$^{V943F/+}$ lines, complementary single-stranded oligodeoxynucleotides (ssODNs) were designed as custom synthetic genes (Megamer single-stranded Gene Fragments, IDT) including these point mutations. sgRNAs sequences were selected using Breaking-Cas[41] and the CRISPOR-TEFOR online tool.[42] The *Cas9* mRNA and sgRNAs templates were amplified by polymerase chain reaction (PCR) with the addition of the SP6 and T7 promoters, respectively, and assembled in the pX330 plasmid.[43] *Cas9* mRNA was transcribed using the mMESSAGE mMACHINE SP6 Transcription Kit (Invitrogen, AM1340), sgRNAs were transcribed with the Megashortscript T7 trancription Kit (Invitrogen, AM1354), and all species were purified on NucAway Spin Columns (Ambion, AM10070). The final concentration of components was 30 pmol/μL sgRNA, 30 ng/μL Cas9 mRNA, and 30 or 10 ng/μL ssODN, as detailed in Table S1, sheets 1 and 2. The sgRNA and ssODN sequences used are listed in Table S1, sheet 1. Reagents were microinjected into 1-cell fertilized C57BL/6 mouse embryos.[44] Pups were screened for the targeted mutation or insertion by PCR analysis and sequencing, and the selected founders were backcrossed to the C57BL/6 background.

Triple mutant mice were obtained by microinjecting the editing reagents for each combination into zygotes obtained from crosses between *Mib1* mutant males (Mib$^{V943F/V943F}$ or Mib$^{R530X/+}$)

and C57Bl/6Crl females, with synthetic crRNA and tracrRNA incubated with Cas9 protein and ssODN at the concentrations indicated in Table S1, sheet 3. Complementary and asymmetric ssODNs (Table S1, sheet 1) were designed according to published guidelines[45] as custom synthetic genes (Megamer single-stranded Gene Fragments, IDT). Founders were identified by PCR and confirmed by Sanger sequencing. Single and multiple mutants were obtained for all microinjections except for the second Cep192+Tmx3 experiment, in which no pup was born. In a second experiment with these reagents, we obtained 1 triple heterozygote founder (Mib1$^{V943F/+}$ Cep192$^{T1522M/+}$ Tmx3-204$^{F191X/+}$) out of 4 survivors (25%). In the Bcl7a microinjection experiment, with only 1 crRNA and 1 ssODN carrying the intron variants, we obtained 13 founders with both intronic mutations out of 21 pups (61.9%).

For the polymorphisms found in the R530X family, 2 triple heterozygotes (Mib1$^{R530X/+}$ Asxl3$^{M1361V/+}$ Apcdd1$^{V150I/+}$) were obtained out of 16 pups (12.5%) were obtained (Table S1, sheet 3). Founders were crossed with C57Bl/6 mice to dilute possible off-target effects of CRISPR-Cas9 editing. The crosses also allowed us to determine whether the mutations were introduced in *cis* or *trans* heterozygosity. Thus, the generation of single mutants was a rare event because most of the animals were either triple heterozygotes or WT, indicating *cis* heterozygosity (Table S2, sheet 4). Generation of the *cis* triple heterozygote was further confirmed by comparing the number of mice with cosegregating alleles versus the number with mixed markers, which showed that all gene pairs were linked. With the set of mutations associated with the MIB1^{V943F} family, we obtained similar results, although cosegregation was less complete (Table S2, sheet 4). When comparing pairs of genes, no significant difference between mutant and WT alleles was found. In addition, despite the distance between *Tmx3* and *Mib1* (almost 80 Mb), the 3 genes cosegregated. Primers for genotyping and expression analyses are provided in Table S3.

Transgenic R26MIB1$^{V943F/+}$ and R26MIB1$^{WT/+}$ mice were generated by homologous recombination in mouse embryonic stem cells. The HA-MIB1^{WT}-IRES-eGFP and HA-MIB1^{V943F}-IRES-eGFP constructs were obtained from pCDNA3.1-HA-MIB1$^{WT\ or\ V943F}$-IRES-eGFP,[34] cloned into pBigT (Addgene, plasmid 15037) and loxP-flanked. *PGK-Neo^{R}STOP*-MIB1^{WT}-EGFP or -MIB1^{V943F}-EGFP expression cassettes were cloned into a modified version of the *pROSA26-1* plasmid (Figure S3A). Gene targeting of these 2 constructs was performed in G4 mouse embryonic stem cells and confirmed by Southern blotting with external 5′ and 3′ hybridization probes (Figure S3B). Mice were generated by injecting targeted cells into B6CRL blastocysts to generate chimeras that were then analyzed for germline transmission. The selected animals were backcrossed to the C57BL/6 background.

LVNC Clinical Phenotype Evaluation

We included patients with an echocardiographic diagnosis of LVNC, defined by the presence of at least 3 prominent trabeculations in the left ventricle and a ratio of noncompacted to compacted segment >2.0 at end-diastole.[46,47]

Exome Sequencing and Data Analysis

DNA was sequenced on Illumina HiSeq2500 or Illumina HiSeq3000 platforms. Variant discovery was performed using Genome Analysis Toolkit (GATK) Best Practices Workflows for germline short variants version 3.7[48] and bundle reference files for genome version b37/GRCh37. For data pre-processing, quality trimming and adaptor removal were performed using Trimmomatic 0.38[49] in paired mode (ILLUMINACLIP:TruSeq3-PE.fa:2:30:10). Low quality bases from the beginning and end of the read pair were deleted if the score was <3 (LEADING:3 TRAILING:3) or if the average quality was <15 using a sliding window of size 4 for the whole read (SLIDINGWINDOW:4:15). The read pair was discarded if the posttrimming length was <36 bp (MINLEN:36). Reads were mapped to GRCh37/b37 human genome using BWA mem version 0.7.10-r789 with shorter split hits set as secondary (*-M*).[50] Reads originating from the same DNA fragment (duplicates) during library construction were identified with Picard v1.97 (MarkDuplicates). For reads obtained from HiSeq 2500 runs (unpatterned flowcell), the maximum offset between 2 duplicated clusters parameter (*OPTICAL_DUPLICATE_PIXEL_DISTANCE*) was set to 100, and reads obtained from HiSeq3000 (patterned flowcell) were set to 2500. The base quality score of bases was recalibrated to better account for systematic errors using the BaseRecalibrator tool in GATK 3.7. The following databases of known polymorphic sites (-knownSites) were used: 1000G_phase1.snps.high_confidence.b37.vcf.gz;Mills_and_1000G_gold_standard.indels.b3 7.vcf.gz and dbsnp_137.b37.vcf.gz. For each sample, intermediate gVCF files with single nucleotide polymorphisms (SNPs) and Indels calls were created for each sample independently using GATK HaplotypeCaller, restricting calling regions to the enrichment targeted regions (L). "SureSelect Human All Exon V6" target intervals were downloaded from Agilent (https://www.agilent.com).

Joint genotyping from gVCF files was performed using the GenotypeGVCFs tool in GATK 3.7. Variants were annotated using the VEP (Variant Effect Predictor) in ensembltools version 84 with the plugin modules LoFtool and CADD (version 1.3) in offline cache version 90.[51] For each putative variant, a variant quality score log-odds (VQSLOD) score was calculated using the VariantRecalibrator and ApplyRecalibration tools in GATK 3.7. SNPs and Indels were treated separately. For SNPs (-mode SNP), QualByDepth (QD), RMSMappingQuality (MQ), MappingQualityRankSumTest (MQRankSum), ReadPosRankSumTest (ReadPosRankSum), FisherStrand (FS), and StrandOddsRatio (SOR) covariates were annotated. In addition, hapmap_3.3.b37.vcf.gz was set as both a truth and a training set (prior 15.0). 1000G_omni2.5.b37.vcf.gz and 1000G_phase1.snps.high_confidence.b37.vcf.gz were set as training sets (prior 12.0 and 10.0, respectively). dbsnp_137.b37.vcf.gz was set as a known set (prior 2.0). For Indels (-mode INDEL), the max number of Gaussians for the positive model (-maxGaussians) was set to 4. QualByDepth (QD), FisherStrand (FS), StrandOddsRatio (SOR), MappingQualityRankSumTest (MQRankSum), and ReadPosRankSumTest (ReadPosRankSum) covariates were annotated.

Mills_and_1000G_gold_standard.indels.b37.vcf.gz was set both as truth and a training set (prior 12), and dbsnp_137.b37.vcf.gz was set as a known set (prior 2.0). In both cases, the truth sensitivity level was set to 75 (--ts_filter_level) to achieve a Ti/Tv ratio close to the expected value for WES (2.8). Because family pedigree data were insufficiently sensitive to allow dismissal of Mendelian inconsistencies as presumable

false positives, we did not use VQSLOD for filtering (although we did use it as for accuracy guidance). The total number of variants identified and proportion of them present in dbSNP as a readout of homogeneity and quality are shown in Table S10.

Cosegregating Variants Filtering

Our workflow is summarized in Figure S4. After obtaining the raw reads and filtering out the low-quality sequences, we mapped the reads to the reference human genome version GRCh37. These mapped reads were handled according to GATK best practices.[52,53] For the MIB1^{R530X} family, of 1341 variants present in an autosomal dominant pattern cosegregating with LVNC, we had data for all the family members of 106 SNPs. These 106 variants affected 21 unique genomic positions, and filtering out low impact and UTR-affecting polymorphisms, 15 candidates were further examined. In the MIB1^{V943F} family, we found 1963 variants inherited in an autosomal dominant fashion, of which 565 were sequenced in all samples. Of the 77 unique positions affected, 32 were not variants of low impact or affecting UTRs. Candidate variants were selected through 3 approaches. First, we performed filtering on the basis of variants. We used databases such as ClinVar[54] to determine if the identified candidate variants were already described in congenital heart disease, but found none already related to LVNC but MIB1^{R530X} and MIB1^{V943F}. We also examined the prevalence of the polymorphisms and their presence in the homozygous condition in gnomAD,[55] although they were not excluding criteria, given how rare *MIB1* mutations are and our hypothesis of the cosegregation of additional mutations. The highest frequency of the selected variants was 0.21 for TMX3^{F191X} (Figure S6C). Another criterion was their predicted functional effect, based on the nature of the mutations, how deleterious were they predicted to be, using CADD[56] (ex post cutoff value: 0.771), PolyPhen (0),[57] and genomic evolutionary rate profiling (GERP)[58] (−3.92), or the potentially affected domain (based on PFAM, PROSITE, etc).[51] These criteria did not allow us to exclude any variant, but were useful to prioritize them for the next 2 approaches. Second, we used a gene-centered strategy. We searched several gene databases for information about the relationship of the variants to congenital heart disease,[59] their annotation in Cardiovascular Gene Ontology,[60] and their expression during heart development (https://www.ncbi.nlm.nih.gov/sra[61,62]). Third, we used haplotypes mapping. We looked for rare variants inherited together in affected relatives using variants themselves (Rare Heterozygous Rule Out) or region markers (Identity-By-Descent or Collapsed Haplotype Patterning[63]).

TMX3 Variants Analysis

The identified *TMX3* mutation (c.637+16_367+17del) affects intron 9 of the main isoform (*TMX3-201*), but also generates a nonsense mutation at Phe191 (TTT) in isoform TMX3-202, located in exon 8. This is equivalent to exon 8 and part of intron 9 in *TMX3-201*, because alternative splicing discards exon 6. The *TMX3-201* nonsense mutation deletes Ts 2 and 3 from the codon, creating a stop codon through combination with the As in the subsequent Asp192 codon (AAC). The remaining protein coding isoform, *TMX3-204*, consists of the first 8 exons of the main isoform with an alternative 3' end fragment including part of *TMX3-201* intron 8. This third isoform encodes a VIFKI sequence in a fragment of intron 8, as well as including a Phe191 (TTT) followed by Lys192 (AAA). The c.579+8_c.579+9_del deletion, analogous to that generating TMX3 (thioredoxin related transmembrane protein 3)-202^{F191X}, would therefore cause a similar nonsense mutation in TMX3204 (Figure S6E). Although the DNA sequence is conserved at that amino acid position, the mouse sequence contains a previous stop codon (Q189X). Mouse homologs of the *TMX3-202* and *TMX3-204* isoforms have not been annotated. To determine if the mouse heart expresses a *Tmx3-204* isoform, we designed 2 primer pairs for RT-PCR. One forward primer (long) binds to exon 6; the other (short) is homologous to a sequence in exon 7. The shared reverse primer binds to the putative 3'UTR, located in intron 8 of the main isoform, and allowed us to amplify *Tmx3-204* alone. RT-PCR with RNA from whole E14.5 hearts showed transcription of this mRNA species in the mouse (Figure S6F).

Additional methods are detailed in the Supplemental Material.

RESULTS

Mib1^{R530X} and Mib1^{V943F} Mutations Cause LVNC and BAV

To assess the consequences of the MIB1^{R530X} and MIB-1^{V943F} mutations previously identified in LVNC families,[34] we generated mice harboring the orthologous nonsense and missense variants by CRISPR-Cas9 gene editing (Figure S1A and S1B, Table S1, sheets 1 and 2). Homozygous Mib1^{R530X} mutants died at embryonic day (E) 11 (Table S2, sheet 1) with severe growth retardation and defective heart looping (Figure 1A through 1A"), reduced NOTCH1 (NOTCH receptor 1) activity (Figure 1B through 1C"), and impaired trabeculation and ventricular patterning (Figure S1C through S1J). Quantitative PCR analysis showed a severely reduced *Mib1* transcription in E10.5 homozygous Mib1^{R530X} mutants (Figure S1K). Heterozygous Mib1$^{R530X/+}$ mice were born at the expected Mendelian ratio and did not show LVNC (Table S2, sheet 1, Figure S2A and S2B).

During compaction, MIB1 regulates myocardial NOTCH-ligand signaling to the endocardium.[10,34] To specifically abrogate MIB1 in the myocardium, we generated Mib1$^{R530X/flox}$;Tnnt2^{Cre} mice. These mice developed severe LVNC by E16.5 (Figure 1D through 1E", Figure S2C and S2D), with a 45% thinning of the compact myocardium, deep endocardial recesses, a reduced compact-to-trabecular myocardium ratio (Figure 1E"'), and attenuated NOTCH1 activity (Figure 1C" and 1F through 1G"). Only 5% of Mib1$^{R530X/flox}$;Tnnt2^{Cre} mice reached adulthood (Table S2, sheet 2), suggesting that the combination of myocardial MIB1 abrogation with global MIB1 haploinsufficiency compromises viability ($P<0.0001$, 2-tailed binomial test). Indeed, Western blot (WB) analysis revealed a drastically reduced MIB1 expression in Mib1$^{R530X/flox}$;Tnnt2^{Cre} hearts (Figure S2E). Ultrasound analysis of surviving adult mice revealed the

ORIGINAL RESEARCH ARTICLE

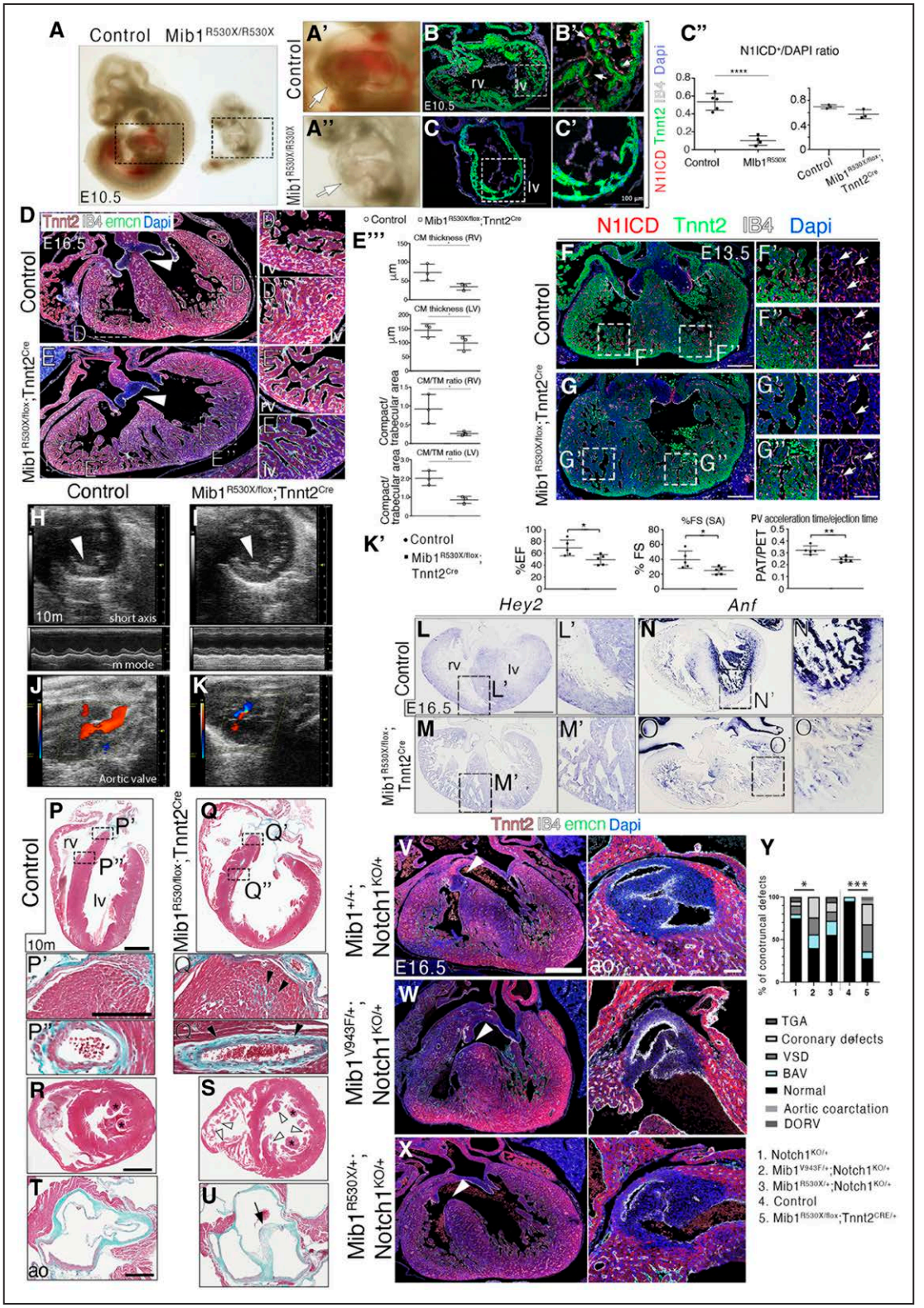

Figure 1. Mib1^{R530X} and Mib1^{V943F} mutations cause LVNC or BAV in a sensitized NOTCH1-deficient genetic background. **A**, Whole mounts of E10.5 control (**left**) and Mib1$^{R530X/R530X}$ mouse embryos (**right**). High-magnification views of the boxed areas show a lateral aspect of a control looped heart (**A'**) and a dysmorphic unlooped mutant heart (**A''**). **B** through **C'**, E10.5 control and Mib1$^{R530X/R530X}$ hearts immunostained for N1ICD (red), Tnnt2 (green), and IB4 (isolectin B4; white). Nuclei are counterstained with DAPI. Arrows point to positive nuclei. Scale bars, 100 µm (**B** and **C**) and 50 µm (**B'** and **C'**). **C''**, **Left**, Quantification of N1ICD staining. Data are mean±SD (n=3 sections from 5 control and n=3 sections from 4 mutant embryos, ****P<0.0001 by Student t-test). **D** and **E**, E16.5 control (**D** through **D''**) and Mib1$^{R530X/flox}$;Tnnt2^{Cre} (**E** through **E''**) transverse heart sections immunostained for Tnnt2 (red), IB4 (white), and emcn (endomucin, green), (*Continued*)

Figure 1 Continued. and counterstained with DAPI. General views and high-magnification views of right and left ventricles (**D'** and **D"**) show the reduction in compact myocardium thickness in mutant embryos (**E'** and **E"**). Scale bar, 200 µm. **E"'**, Quantification of compact myocardium (CM) thickness and the CM-to-trabecular myocardium (TM) ratio in both ventricles. Data are mean±SD (each point represents the average of 3 sections of each animal, 3 control and 3 mutants $^{**}P<0.005$ by Student *t*-test). **F** through **G"**, E13.5 control (**F**) and Mib1$^{R530X/flox}$;Tnnt2^{Cre} (**G**) transverse heart sections immunostained for N1ICD (red), Tnnt2 (green), and IB4 (white) and counterstained with DAPI. General views and insets of right (**F'** and **G'**) and left (**F"** and **G"**) ventricles. Arrows point to positive nuclei. Scale bar, 50 µm. **C"**, **Right**, Quantification of N1ICD staining. Data are mean±SD (n=3 sections from 5 WT and n=3 sections from 4 mutant embryos, $P<0.0585$, by Student *t*-test). **H** through **K**, Ultrasound short axes and M-mode views of 10-month-old control and Mib1$^{R530X/flox}$;Tnnt2^{Cre} ventricles. **H** and **I**, Arrowheads indicate the smooth surface of the control left ventricle and the trabeculae in the Mib1$^{R530X/flox}$;Tnnt2^{Cre} left ventricle. **J** and **K**, Color flow imaging of control and Mib1$^{R530X/flox}$;Tnnt2^{Cre} hearts showing regurgitation through the aortic valve in the mutant. **K'**, Quantification of ejection fraction (EF), fractional shortening (FS), and the pulmonary vein acceleration time-to-ejection time ratio. Data are mean±SD (n=5 WT and n=5 mutants, $^{*}P<0.05$ and $^{**}P<0.01$, Student *t*-test). **L** through **O'**, ISH in E16.5 control and Mib1$^{R530X/flox}$;Tnnt2^{Cre} heart sections. *Hey2* expressed in compact myocardium (**L** through **L'**) is expanded to trabeculae in mutants (**M** through **M'**), whereas the trabecular marker *Anf* (**N** through **N'**) is weakly expressed in mutant trabeculae (**O** through **O'**). Scale bar, 200 µm. **P** through **U**, Trichrome acid staining of 10-month-old adult control and Mib1$^{R530X/flox}$;Tnnt2^{Cre} heart sections. **P** and **Q**, Four-chamber view. Note the dilated mutant heart (**Q**). High-magnification views of boxed areas show details of the ventricular septum (**P'** and **Q'**) and coronary vessels (**P"** and **Q"**). **R** and **S**, transverse heart sections. Papillary muscles are marked with an asterisk. Arrowheads point to trabeculae in mutant heart (**S**). **T** and **U**, Section at the level of aortic valves. Arrow points to a dysplastic BAV in mutant heart. Scale bars, 1 mm and 400 µm. **V** through **X**, Transverse heart sections and aortic valves from E16.5 Mib1$^{+/+}$; Notch1KO/+ (**V**), Mib1V943F/+; Notch1KO/+ (**W**), and Mib1R530X/+; Notch1KO/+ (**X**) embryos immunostained for Tnnt2 (red), IB4 (white) and emcn (green), and counterstained with DAPI. Arrowheads mark the membranous ventricular septum, which is defective in Mib1$^{V943F/+}$; Notch1$^{KO/+}$ and Mib1$^{R530X/+}$; Notch1$^{KO/+}$ hearts. Sections on the **right** show the aortic valves, which are bicuspid in the hearts of double heterozygotes. Scale bar, 100 µm. **Y**, Quantification of conotruncal defects. Data are mean±SD (n=18 N1$^{KO/+}$, n=24 Mib1$^{V943F/+}$; Notch1$^{KO/+}$, n=16 Mib1$^{R530X/+}$; Notch1$^{KO/+}$, n=22 control and n=18 Mib1$^{R530X/flox}$;Tnnt2^{Cre}; $^{*}P<0.05$, $^{***}P=0.0003$, Fisher exact test for the proportion of abnormal hearts). ao indicates aortic valve; BAV, bicuspid aortic valve; E, embryonic day; lv, left ventricle; LVNC, left ventricular noncompaction; N1ICD, NOTCH1 intracellular domain; NOTCH1, NOTCH receptor 1; rv, right ventricle; Tnnt2, cardiac troponin T; and WT, wild-type.

presence of trabeculations and a significant reduction in ejection fraction and fractional shortening, indicating impaired cardiac function (Figure 1H, 1I, and 1K'). In addition, color Doppler profiling detected regurgitation through the aortic valve in mutant mice (Figure 1J and 1K). Developmental analysis of chamber markers in E16.5 Mib1$^{R530X/flox}$;Tnnt2^{Cre} embryos revealed expansion of the compact myocardium marker *Hey2* to the trabeculae (Figure 1L through 1M') and low expression of the trabecular marker *Anf* (Figure 1N through 1O'), indicating altered chamber myocardium patterning in Mib1$^{R530X/flox}$;Tnnt2^{Cre} mutants. Masson trichrome-stained sections of adult hearts revealed myocardial fibrosis in the septum and around the coronary vessels of the dilated Mib1$^{R530X/flox}$;Tnnt2^{Cre} ventricles (Figure 1P through 1Q"). Transverse heart sections revealed the presence of noncompacted trabeculae in Mib1$^{R530X/flox}$;Tnnt2^{Cre} ventricles (Figure 1R and 1S). It is interesting that the adult aortic valve was dysplastic in Mib1$^{R530X/flox}$;Tnnt2^{Cre} mutants (Figure 1T and 1U), suggesting that aortic valve morphogenesis is sensitive to MIB1 dosage.

Heterozygous Mib1$^{V943F/+}$ and homozygous Mib1$^{V943F/V943F}$ mice did not develop LVNC (Figure S2H and S2I) and were viable (Table S2, sheet 3). To test the sensitivity of the LVNC phenotype to NOTCH gene dosage, we introduced a *Notch1* loss-of-function allele (Notch1^{KO})[40] into the Mib1^{V943F} background. Surprisingly, E16.5 Mib1$^{V943F/+}$;Notch1$^{KO/+}$ double heterozygotes mice had highly penetrant BAV and multiple associated valve defects (Figure 1V, 1W, and 1Y, Figure S2J through S2O, Table S4, sheet 1) but not LVNC. Valve defects were not substantial in Mib1$^{R530X/+}$;Notch1$^{KO/+}$ hearts (Figure 1X and 1Y, Table S4, sheet 1), but severe MIB1 depletion in Mib1$^{R530X/flox}$;Tnnt2^{Cre} mice caused BAV and additional conotruncal defects (Figure 1Y, Figure S2F and S2G, Table S4, sheet 1).

We generated 2 transgenic lines bearing a Rosa26-floxNeoSTOPflox-MIB1^{WT}-EGFP or a Rosa26-floxNeoSTOPflox-MIB1^{V943F}-EGFP expression cassette, resulting in conditional expression of a wild-type or a mutant (MIB1^{V943F}) MIB1 (Figure S3 A and S3B). To monitor transgene expression, we crossed these lines with mice harboring the Nkx2.5^{Cre} driver line, which is active in cardiac progenitors from E7.5.[38] CRE-mediated removal of the floxed NeoSTOP sequences resulted in *Rosa26*-driven MIB1^{V943F}-EGFP expression in the E9.0 heart (Figure S3C). To examine the effect of MIB1^{V943F} expression on compaction, we used the MYH6^{Cre} driver, expressed in the developing chamber myocardium from E10.5 onwards.[37] The hearts of mice expressing wild-type MIB1 in the myocardium were normal at E15.5, whereas mice expressing MIB1^{V943F} had thinner compact myocardium and persistent trabeculae compatible with LVNC (Figure S3D through S3F). These results indicate that the Mib1^{R530X} and Mib1^{V943F} mutations impair both chamber and valve development, leading to LVNC and BAV in specific genetic configurations.

MIB1 Is Required for Myocardial Differentiation and Metabolic Maturation

To gain mechanistic insight, we performed RNA-seq on E15.5 Mib1R530X$^{/flox}$;Tnnt2^{Cre} and control ventricles followed by gene set enrichment analysis against "HALLMARK" gene sets (Figure 2A, Table S5, sheets 1 through 6). "EPITHELIAL_TO_MESENCHYMAL_TRANSITION" (EMT) was the highest positively enriched gene set in Mib1$^{R530X/flox}$;Tnnt2^{Cre} mutants (Figure 2A and 2B,

ORIGINAL RESEARCH ARTICLE

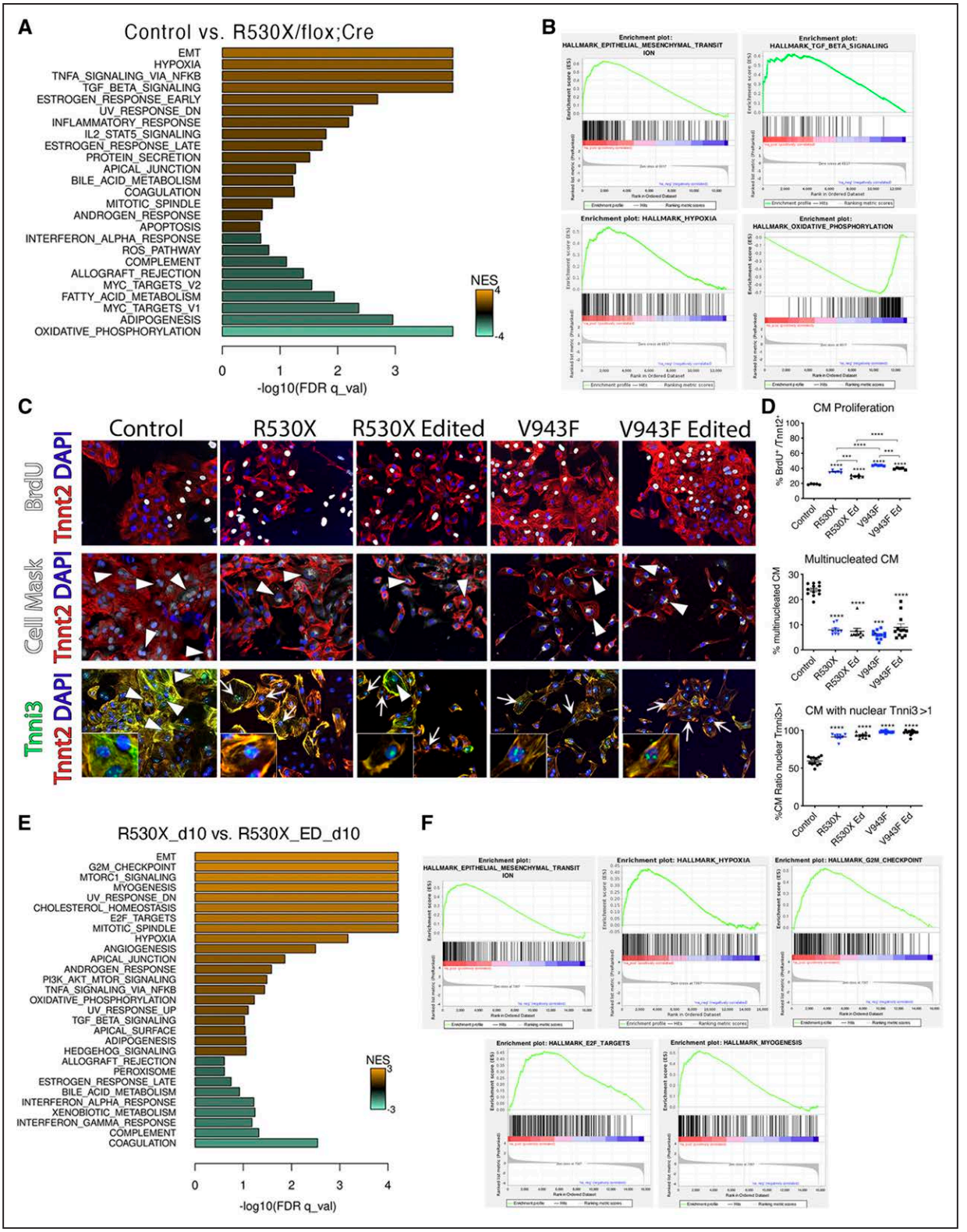

Figure 2. Defective cardiomyocyte differentiation and metabolic maturation in Mib1$^{R530X/flox}$;Tnnt2$^{Cre/+}$ mice and MIB1$^{R530X/+}$ hiPSC-derived cardiomyocytes.

Gene set enrichment analysis (GSEA) of Mib1$^{R530X/flox}$;Tnt2^{Cre} (R530/flox;Cre) and control expression profiles. **A**, Bar plot representing enrichment data for 25 gene sets at false discovery rate (FDR qval) <0.25. Of these, 15 had an FDR qval <0.05. Scale bar indicates the Normalized Enrichment Score (NES) from −4 to 4. Positive and negative scores were found for 16 and 9 gene sets, respectively. **B**, Gene enrichment profiles for "HALLMARK" gene sets "EPITHELIAL_MESENCHYMAL_TRANSITION" (FDR qval=0; NES=2.54), "TGF_BETA_SIGNALING" (FDR qval=0; NES=2), "HYPOXIA" (FDR qval=0; NES=2.15), and "OXIDATIVE_PHOSPHORYLATION" (FDR qval=0; NES=−2.88). (*Continued*)

Figure 2 Continued. C, Cardiomyocytes derived from control, MIB1$^{R530X/+}$, edited MIB1$^{R530X/+}$, MIB1$^{V943F/+}$, and edited MIB1$^{V943F/+}$ hiPSCs after 20 days of differentiation. Cells were stained with antibodies against BrdU (white), Tnnt2 (red), and Tnni3 (green) and counterstained with DAPI (**top** and **bottom** rows), or DAPI and CellMask (blue and white, **middle** row). The **top** row shows increased BrdU staining in cells derived from the patients; the **middle** row shows less multinucleated mature cardiomyocytes in the patients' cardiomyocites (arrowheads); the **bottom** row shows predominant Tnni3 staining in the nuclei of mutant hiPSC-CMs. **D**, Quantification of BrdU incorporation, percentage of multinucleation, and percentage of nuclear Tnni3 (see Supplemental Material). Data are mean±SD (n=5 or 6 proliferation; n=9–12 multinucleation/maturation). *p-value* ***<0.005****, *p-value*<0.001, 1-way ANOVA, Tukey multiple comparisons test. **E**, GSEA of R530X_d10 versus R530X_ED_d10 expression profiles. Bar plot representing enrichment data for 29 gene sets at FDR qval <0.25. Of these, 16 had FDR qval <0.05. Scale bar indicates NES from −3 to 3. Positive and negative scores were found for 20 and 9 gene sets, respectively. **F**, Gene enrichment profiles for "HALLMARK" gene sets "EPITHELIAL_MESENCHYMAL_TRANSITION" (FDR qval=0; NES=2.46), "HYPOXIA" (FDR qval=6.13E-04; NES=1.95), "G2M_CHECKPOINT" (FDR qval=0; NES=−2.39), "E2F_TARGETS" (FDR qval=0; NES=2.10), and "MYOGENESIS" (FDR qval=0; NES=2.31). hiPSC indicates human induced pluripotent stem cell; hiPSC-CM, hiPSC-derived cardiomyocytes; Tnnt2, cardiac troponin T; and Tnni3, cardiac troponin I.

Table S5, sheets 1 and 3). Related to this pathway are "TGF BETA SIGNALING", "APICAL_JUNCTION", and "MITOTIC_SPINDLE" (Figure 2A and 2B, Table S5, sheets 1 and 4), suggesting activation of cell migratory processes involving oriented cell division as those occurring in cardiomyocytes during chamber development.[64,65] Prominent cellular stress responses such as "HYPOXIA", "TNFA_SIGNALING_VIA_NFKB","UV_RESPONSE_DN", "INFLAMMATORY_RESPONSE", and "IL2_STAT5_SIGNALING", were also enriched positively and might involve "APOPTOSIS" as a final common pathway (Figure 2A and 2B, Table S5, sheets1 and 5). Conversely, the most negatively enriched pathway was "OXIDATIVE_PHOSPHORYLATION" (Figure 2A and 2B, Table S4, sheets 2 and 6). Related to this pathway are FATTY_ACID_METABOLISM" and "ROS_PRODUCTION" (Figure 2A), suggesting defective cardiac metabolic maturation. Pathways involved in protein homeostasis such as "MYC_TARGET_V1", "MYC_TARGET_V2", and "PROTEIN_SECRETION" were also enriched in Mib1$^{R530X/flox}$;Tnnt2^{Cre} mutants (Figure 2A, Table S5, sheets 1 and 2).

hiPSC-CMs Show Maturation Impairment and Enhanced Proliferation

To determine the cellular phenotype of disease-affected cardiomyocytes, we generated hiPSCs by retroviral transduction of reprogramming factors in skin fibroblasts obtained from MIB1$^{V943F/+}$ and MIB1$^{R530X/+}$ LVNC family members (Figure 3C and 3D; see Methods). Using CRISPR-Cas9 editing, we reverted both *MIB1* mutations to obtain hiPSC isogenic controls. These hiPSC lines were differentiated in vitro into cardiomyocytes.[66] Tnnt2 expression in MIB1$^{V943F/+}$ and MIB1$^{R530X/+}$ hiPSC-CM confirmed similar differentiation efficiency in all lines (Figure 2C and 2D). Human and mouse studies have shown an association between altered proliferation of ventricular cardiomyocytes and the pathogenesis of LVNC,[25,67] with persistent proliferation reported in mouse MIB1-deficient trabecular cardiomyocytes.[34,68] We assessed the proliferative potential of control and MIB1-mutant induced pluripotent stem cell (iPSC)-CMs by measuring BrdU incorporation. We found significantly elevated proliferation in MIB1$^{V943F/+}$ and MIB1$^{R530X/+}$ hiPSC-CMs (Figure 2C and 2D). In addition, MIB1-mutant hiPSC-CMs showed reduced multinucleation and a predominantly nuclear, rather than cytosolic, distribution of Tnni3 (cardiac troponin I) (Figure 2C and 2D), an indication of immaturity.[69]

We performed RNA-seq in mutant (MIB1$^{R530X/+}$, named R530X) and gene-edited (R530X_ED) patient hiPSC lines at day 10 of cardiomyocyte differentiation (Figure 2E). Enrichment against "HALLMARK" gene sets revealed "EMT" as the most positively enriched gene set (Figure 2E and 2F, Table S6, sheets 1 and 3), consistent with in vivo findings in mice. The cellular stress pathways "UV_RESPONSE_DN", "HYPOXIA", and "UV_RESPONSE_UP" (Figure 2E, Table S6, sheets 1 and 4) were also enriched. Enrichment of "G2M_CHECKPOINT" (Figure 2E and 2F, Table S5, sheets 1 and 5) and "E2F_TARGETS" (Figure 2E and 2F, Table S6, sheets 1 and 6), supports deregulation of cell cycle progression and the observed increased in proliferation of R530X hiPSC-CMs (Figure 2C and 2D). MIB1$^{R530X/+}$ hiPSC-CMs displayed altered protein and lipid metabolisms reflected in "MTORC1_SIGNALING", PI3K_AKT_MTOR_SIGNALING", "MYOGENESIS" (Figure 2E and 2F, Table S6, sheets 1 and 7), and "CHOLESTEROL_HOMEOSTASIS", "ADIPOGENESIS", "BILE_ACID_METABOLISM", "XENOBIOTIC_METABOLISM" and "PEROXISOME" (Figure 2E, Table S6, sheet 1), respectively. Conversely, downregulation of several immunohematological processes (Figure 2E, Table S6, sheet 2) suggests impaired processes of innateimmunological recognition.

Multiple Genetic Variants Cosegregate With *MIB1* and LVNC

Individuals heterozygous for the MIB1^{R530X} and MIB-1^{V943F} mutations in our pedigrees show fully penetrant LVNC (Table S7) with characteristic heart dilatation and trabeculations (Figure 3A). The absence of disease in mice heterozygous for these *Mib1* mutations prompted us to perform a WES of these families. We hypothesized that additional genetic variants may cosegregate with the *MIB1* mutations and contribute to the manifestation of the LVNC phenotype in a heterozygous setting. Briefly, variants were filtered using several quality parameters

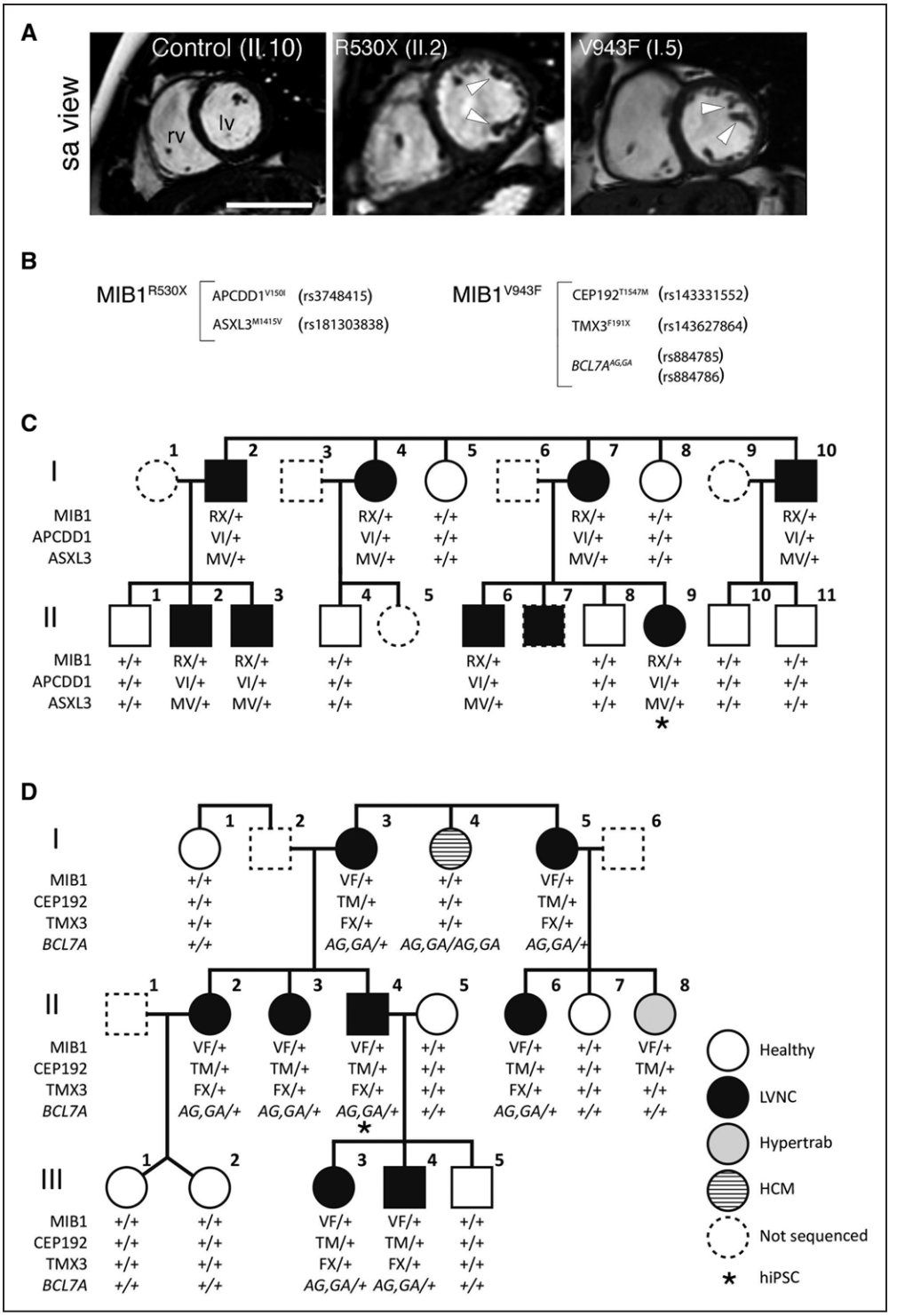

Figure 3. Identification of variants segregating with *MIB1* mutations in human LVNC families by whole exome sequencing.
A, CMRI heart sections showing short axis (sa) views of the right and left ventricles of a control individual (II.10) and patients II.2 and I.5, carrying the MIB1$^{R530X/+}$ and MIB1$^{V943F/+}$ mutations, respectively. Arrowheads point to trabeculae. Scale bar, 50 mm. **B**, Genetic variants associated with the MIB1$^{R530X/+}$ and MIB1$^{V943F/+}$ mutations. Corresponding reference SNP (rs) report references are shown in parentheses. **C**, MIB1$^{R530X/+}$ pedigree. Note the perfect cosegregation of the MIB1$^{R530X/+}$ mutation with the newly identified variants and LVNC. **D**, MIB1$^{V943F/+}$ pedigree. Note the cosegregation of the MIB1$^{V943F/+}$ mutation with the newly identified variants and LVNC. Members of each generation are indicated numerically. Squares, males; circles, females. Asterisks indicate the individuals from which hiPSCs were generated. CMRI indicates cardiac magnetic resonance imaging; hiPSC, human induced pluripotent stem cell; lv, left ventricle; LVNC, left ventricular noncompaction; rv, right ventricle; and SNP, single nucleotide polymorphism.

and inheritance assumptions on the basis of LVNC affection in the family. Filtered variants (15 in MIB1^{R530X} family and 32 in MIB1^{V943F} family) were analyzed focusing on variant, gene, or haplotype characteristics. Our workflow is summarized in Figure S4, and a detailed description of the filtering process can be found in the Methods.

We identified 2 candidate missense variants in the MIB1^{R530X} family (Figure 3B), occurring in heterozygosis in all affected family members and in none of the healthy relatives (Figure 3C). rs3748415 is a valine-to-isoleucine substitution at position 150 (V150I) in APCDD1 (adenomatosis polyposis coli downregulated 1 protein), a WNT signaling inhibitor.[70] It is interesting that WNT and NOTCH have been shown to genetically interact during cardiac development.[71] The second genetic variant, rs181303838, is a methionine-to-valine substitution in position 1415 (M1415V) in additional sex combs like ASXL3 (transcriptional regulator 3), a transcription factor involved in heart development and homeostasis.[72] Both *APCDD1* and *ASXL3* are physically close to *MIB1* in chromosome 18, increasing the chances of cosegregation (Figure S5A). The mutation found in *APCDD1* alters Val150, which is conserved between zebrafish and humans (Figure S5B) and predicted to be in the top 2.4% of deleterious variants in the genome (CADD Phred 16.26). Met1415 in ASXL3 is a rare variant (minor allele frequency 0.0004467) conserved in all eutherians examined (Figure S5B). Its hydrophobicity is maintained in *Xenopus laevis*'s Leu1368 (Figure S5B). The APCDD1^{V150I} mutation was predicted to be more deleterious than ASXL3^{M1415V} (PolyPhen scores of 0.555 and 0, respectively) and to be more evolutionarily conserved (CADD Phred,16.26 and 8.681; and GERP, 1.79 and −1.58). Nevertheless, APCDD1^{V150I} was more prevalent in human populations (minor allele frequency 0.1611; Figure S5C). Both genes are expressed during mouse ventricular and cardiac valve morphogenesis (E12.5–E16.5). Quantitative PCR of whole hearts from C57Bl/6 embryos from E10.5 to E16.5 demonstrated that *Apcdd1* and *Asxl3* are regulated differentially during this period (P<0.0001 in both cases). The expression of both genes peaks at E12.5 and then declines progressively (Figure S5D).

The first identified variant in the MIB1^{V943F} family (rs143331552) was a threonine-to-methionine substitution at position 1547 (T1547M) of CEP192, which is required for mitotic spindle assembly.[73] The second variant (rs143627864) was a nonsense mutation of the phenylalanine at position 191 (F191X) of thioredoxin-related transmembrane protein 3 (TMX3), which catalyzes the isomerization of protein disulfide bonds.[74] TMX3 mutations have been linked to microphtalmia.[75] The third and fourth variants (c.175-56A>G, rs884785, and c.175-27G>A, rs884786) occur in intron 2 of BAF chromatin remodeling complex subunit BCL7A, which is involved in the pathogenesis of B cell lymphomas.[76] All of these variants appeared in heterozygous combination with MIB1^{V943F} and cosegregated with LVNC (Figure 3D). *CEP192* and *TMX3* are physically linked to *MIB1* on chromosome 18, but *BCL7A* is not. In humans, *CEP192* is located on the short arm of chromosome 18, close to *MIB1*. In mice, this gene is farther away, in a translocated region of the long arm. In both species, *TMX3* is located at the end of the long arm, almost 50 Mb away from *MIB1* in humans and 80 Mb away from *Mib1* in mice. *BCL7A* is located on human chromosome 12. In mice, *Bcl7a* is located on the long arm of chromosome 5 (Figure S6A). The T1547M variant of the CEP192 gene is rare (maximum minor allele frequency 0.00003). PolyPhen identifies it as possibly damaging (Polyphen, 0.658), and CADD predicts it to be among the 1.45% most deleterious variants (CADD Phred score, 18.39). Thr1547 is in a highly conserved region of the CEP192 amino acid sequence in zebrafish and all Tetrapoda (Figure S6B). Both intron mutations in *BCL7A* are conserved between zebrafish and humans (Figure S6B). The CADD Phred scores for the *BCL7A* intron variants were low (6.350 and 0.771), as were the GERP scores (−3.88 and −3.92). The GERP score for CEP192^{T1547M} (0.69) was also not high; however, the prevalence of this mutation is sufficiently low (0.00003) to warrant consideration. The *BCL7A* mutations are prevalent (rs884785, 0.11; rs884786, 0.032; Figure S6C). Quantitative PCR analysis showed that these genes are expressed from E10.5 to E14.5, followed by a significant decline in transcription (Figure S6D). The mutated phenylalanine residue in TMX3^{F191X} is subjected to some selective pressure (GERP score: 0.63, Figure S6C), and substitution occurs at a frequency that could fit in LVNC prevalence in combination with any of the other candidate mutations found in the MIB1^{V943F} family (Figure S6E). RT-PCR analysis at E14.5 confirmed that the *TMX3* is expressed in the mouse heart (Figure S6F; see Methods). All these variants, although predicted as benign or of uncertain significance by their effect or prevalence (Figures S5 and S6), are not present simultaneously with their respective *MIB1* variants in any gnomAD HGDP or 1000 genomes[77] individual (Tables S8 and S9).

Heterozygous Combination of *MIB1* Mutations With the *ASXL3* and *APCDD1* or With the *CEP192, TMX3*, and *BCL7a* Variants Causes LVNC or BAV in Mice

To determine whether the newly identified candidate variants contribute to the autosomal dominant inheritance pattern of LVNC in our pedigrees, we used CRISPR-Cas9 gene editing to generate triple (Mib1R530X/+ Asxl3M1361V/+ Apcdd1V150I/+) and quadruple (Mib1V943F/+ Cep192T1522M/+ Tmx3$^{F191X/+}$; Bcl7a$^{AG,GA/+}$) heterozygous mutant mice using gene editing (Figure S7). CRISPR reagents were microinjected into zygotes

of crosses between *Mib1* mutant males (*Mib*$^{V943F/V943F}$ or *Mib*$^{R530X/+}$) and C57BL/6J females (Table S1, sheet 3). We aimed to introduce the new variants in cis with those in *Mib1* because the genes involved are linked, so this would yield a higher frequency of multiple heterozygotes. Founders were identified by PCR and confirmed by Sanger sequencing (Figure S7). For the variants identified in the MIB1^{R530X} family, we obtained 2 triple heterozygotes (Mib1$^{R530X/+}$ Asxl3$^{M1361V/+}$ Apcdd1$^{V150I/+}$) out of 16 (12.5%) animals (Table S1, sheet 3). For those of the MIB1^{V943F} family variants, we obtained 1 triple heterozygote founder (Mib1$^{V943F/+}$ Cep192$^{T1522M/+}$ Tmx3$^{F191X/+}$) out of 4 survivors (25%). In the Bcl7a microinjection, we obtained 13 founders out of 21 pups (61.9%) with both intronic mutations (Table S1, sheet 3). The founders generated were crossed with C57BL/6J mice to dilute any possible off-target effect of CRISPR-Cas9 gene edition. These crosses also allowed us to determine if the mutations were introduced in *cis* or in *trans* heterozygosity. Most of the animals were either triple heterozygotes or wild-type, indicating *cis* heterozygosity. For details, see the Supplemental Material.

Triple heterozygous Mib1$^{R530X/+}$ Asxl3$^{M1361V/+}$ Apcdd1$^{V150I/+}$ mice (abbreviated as *Thet*) reached adulthood and were fertile. At E16.5, the hearts of these mice displayed thinner ventricles and larger but thinner trabeculae than control counterparts, and also had a significantly reduced a compact myocardium:trabeculae area ratio, indicating LVNC (Figure 4A through 4C, Table S4, sheet 2). Cardiac magnetic resonance imaging of adult Mib1$^{R530X/+}$ Asxl3$^{M1361V/+}$ Apcdd1$^{V150I/+}$ mice revealed dilated chambers with elevated end diastolic volume, left ventricular mass, systolic volume, and cardiac output (Figure 4D through 4H). These elevated parameters are compatible with the pathogenesis of high-output heart failure.[78]

We performed RNA-seq at E15.5, followed by gene set enrichment analysis, and identified "DNA_REPAIR" as the most enriched pathway, followed by "MYC_TARGETS_V1" and "E2F_TARGETS" (Figure 4I and 4J, Table S11, sheets 1 through 3), reflecting dysregulation of cell cycle checkpoint controls (G2/M and S phases). We also found enriched the "P53_PATHWAY", an effector of cellular stress pathways including "ROS_PATHWAY", "UNFOLDED PROTEIN RESPONSE", and "UV_RESPONSE (_UP and _DN)" that may act upstream of cell-cycle checkpoints and involve "APOPTOSIS" as an outcome (Figure 4I, Table S11, sheet 1). Enrichment of the "ALLOGRAFT_REJECTION" and "INTERFERON_ALPHA_RESPONSE" terms (Figure 4I, Table S11, sheet 1), may reflect activation of innate immunity pathways. "MTORC1_SIGNALING" enrichment and "PROTEIN SECRETION" depletion suggest that protein homeostasis is likely altered in *Thet* mice (Figure 4I, Table S11, sheets 1 and 6). Given that APCDD1 is a direct WNT signaling target,[70] the enrichment of "WNT_BETA_CATENIN_SIGNALING" (Figure 4I and 4J, Table S11, sheets 1 and 4), is consistent with WNT and NOTCH pathways playing opposite roles during cardiogenesis. "EMT" enrichment (Figure 4I and 4J, Table S11, sheets 1 and 5) is consistent with an increase in cell migratory processes. Defective ventricular development in *Thet* mutants is associated with increased proliferative and migratory processes, defective cellular stress responses, and protein homeostasis, indicative of a maturation defect.

After including our published Mib1$^{flox/flox}$;Tnt2^{Cre} mice gene profile,[34] we performed a comparative analysis of all the gene set enrichment analyses made in this study. We observed that the Mib1$^{R530X/flox}$;Tnnt2^{Cre} signature was more closely related to those of the Mib1$^{flox/flox}$;Tnt2^{Cre} mice and R530X_d10 iPSCs than to that of *Thet* mice (Figure S8). Considering all the pathway overlaps, we found that contrasts showing the strongest enrichments (P<0.05), were Mib1$^{R530X/flox}$;Tnnt2^{Cre} versus control and R530X_d10 versus R530X_ED_d10 iPSCs (Figure S8). Shared pathways included "EMT", "TGF_BETA_SIGNALING", "ESTROGEN_RESPONSE_EARLY", "TNFA_SIGNALING_VIA_NFKB", and "IL2_STA5_SIGNALING" (Figure S8). These pathways were more enriched, with a level of significance at qVal<0.05 or qVal<0.25) in Mib1$^{R530X/flox}$;Tnnt2^{Cre} and R530X_d10 (Figure S8). Depleted pathways (at qVal<0.05 and/or qVal<0.25) involved immune-hematological processes (Figure S8). However, these pathways were either moderately enriched or unchanged in *Thet* mice (Figure S8). Collectively, the RNA-seq data suggest that defective ventricular chamber maturation in *Mib1* mutants is caused by aberrant proliferative, migratory, fibrotic, and inflammatory pathway gene activation. Acting alongside these "primary" pathways are "secondary" pathways, which are enriched or depleted depending on the specific genotype.

Triple heterozygous Mib1V943F/+ Cep192T1547M/+ Tmx3F191X/+ E16.5 mice showed significantly more penetrant valve abnormalities at E16.5, including BAV (Figure 4K through 4N and 4S), as well as defects in both the muscular and the membranous ventricular septum (Table S4, sheet 3). Quadruple heterozygous mutants harboring the Bcl7a variants also had BAV, as well as coronary artery defects (Figure 4O through 4S, Table S4, sheet 3).

We examined the UK Biobank in search of BAV or aortopathy cases with *MIB1* mutations. We found that in the WES cohort of 454756 individuals, 1408 heterozygous participants carried 412 rare predicted loss of function *MIB1* variants (0.3%; 1 in 323), and 3028 participants carried 533 rare missense *MIB1* variants (0.2%; 1 in 853). Eighty-five heterozygous missense variant carriers of 3028 heterozygote individuals were diagnosed with aortic valve disease (0.03%; 1 in 36). Thirty-six heterozygous predicted loss of function variant carriers of 1408 heterozygote individuals were diagnosed with

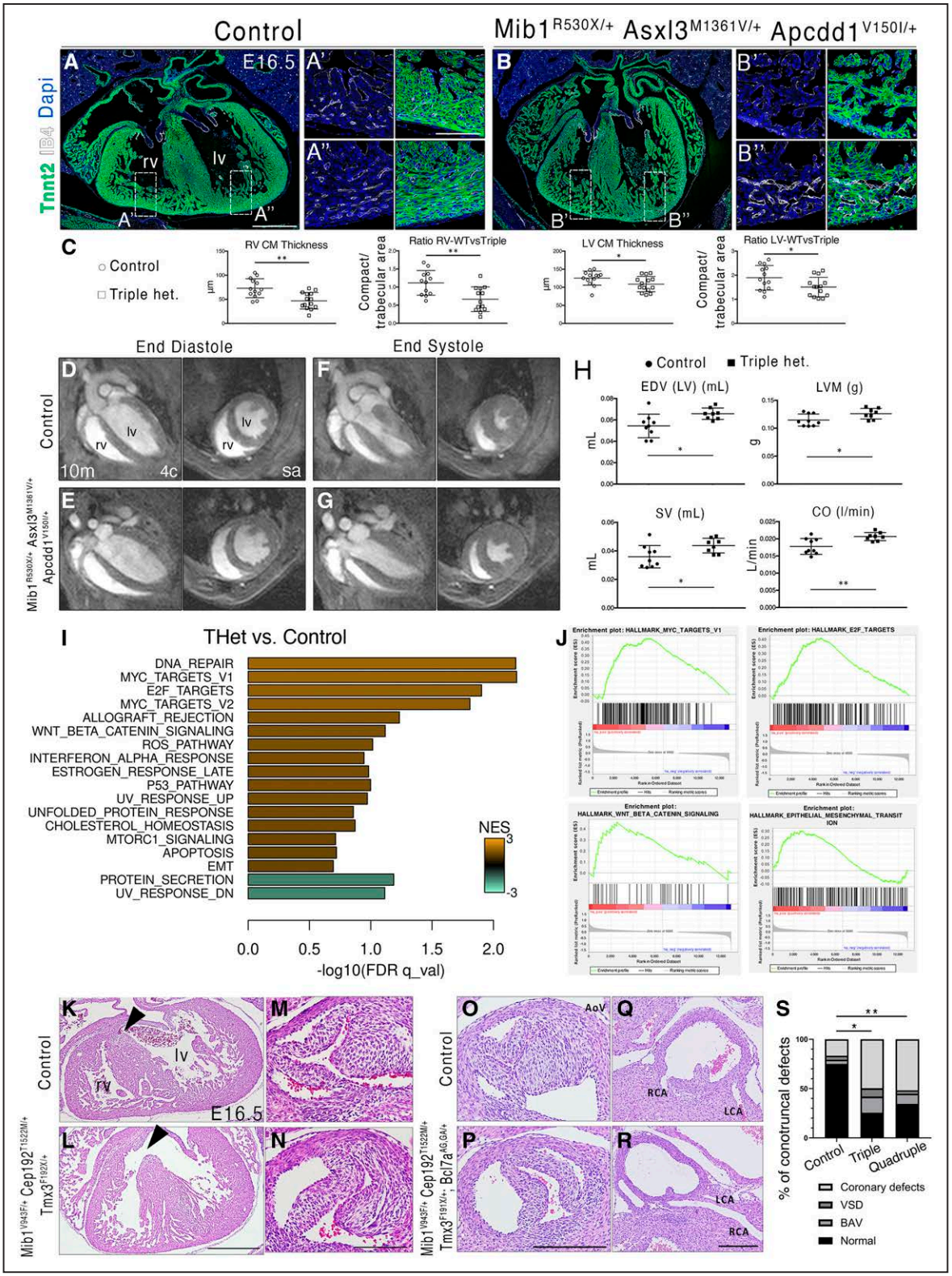

Figure 4. Mib1R530X/+ Asxl3M1361V/+ Apcdd1V150I/+ and Mib1V943F/+ Cep192T1522M/+ Tmx3$^{F191X/+}$:Bcl7a$^{AG,GA/+}$ compound heterozygous mice show LVNC and BAV.

A and **B**, Transverse heart sections from E16.5 control and Mib1$^{R530X/+}$ Asxl3$^{M1361V/+}$ Apcdd1$^{V150I/+}$ embryos stained with antibodies to Tnnt2 (green) and isolectin B4 (white), and counterstained with DAPI (blue). General views of left and right ventricle (**A** and **B**) and high-magnification views of boxed areas (**A'** and **B"**), showing reduced compact myocardium thickness in triple heterozygous embryos. Scale bars, 500 µm (**A** and **B**) and 100 µm (magnifications). **C**, Quantification of compact myocardium (CM) thickness and the compact-to-trabecular myocardium area ratio in both ventricles. Data are mean±SD (n=3 sections from 11 and 1 section from 2 WT and n=3 sections from 11 and 1 section from 3 mutant embryos, *P<0.05 and **P<0.005, by Student t-test). **D** through **G**, CMRI images of adult (10-month-old) control (*Continued*)

Figure 4 Continued. (**D** and **F**) and triple heterozygous (**E** and **G**) mice showing chamber dilation in the mutant. **H**, Quantification of end diastolic volume (EDV), left ventricular mass (LVM), stroke volume (SV), and cardiac output (CO). Data are mean±SD (n=9 WT and n=8 mutants, **P*<0.05 and ***P*<0.01, by Student *t*-test). **I**, Gene set enrichment analysis of E15.5 triple heterozygous (Thet) versus control heart expression profiles. The bar plot represents enrichment data for 18 gene sets at FDR qval <0.25. Of these gene sets, 4 had an FDR qval <0.05. The scale bar is the normalized enrichment score (NES) from −3 to 3. Positive scores were found for 16 gene sets and negative scores for 2 gene sets. **J**, Gene enrichment profiles for the "HALLMARK" gene sets "MYC_TARGETS_V1" (FDR qval=0.006; NES=1.84), "E2F_TARGETS" (FDR qval=0.012; NES=1.75), "WNT_BETA_CATENIN_SIGNALING" (FDR qval=0.076; NES=1.51), and "EPITHELIAL_MESENCHYMAL_TRANSITION" (FDR qval=0.202; NES=1.28). **K** through **R**, Hematoxylin and eosin staining of control (**K** and **O**), triple heterozygote Mib1$^{V943F/+}$ Cep192$^{T1522M/+}$ Tmx3F191X/+ (**L**), and quadruple heterozygote Mib1V943F/+ Cep192T1522M/+ Tmx3F191X/+;Bcl7aAG,GA/+ hearts (**P**). Note the ventricular septal defect (**K** and **L**, arrowhead), BAV (**M** and **N**), and coronary malformations (**Q** and **R**). Scale bars, 500 µm (**K** and **L**), 100 µm (**M** through **P**), and 200 µm (**Q** and **R**). **S**, Quantification of conotruncal defects. Data are mean±SD (n=24 WT, 13 triple and 28 quadruple mutants, **P*<0.05, ***P*<0.01, Fisher exact test for the proportion of abnormal hearts). BAV indicates bicuspid aortic valve; CMRI, cardiac magnetic resonance imaging; E, embryonic day; IB4, isolectin B4; lv, left ventricle; LVNC, left ventricular noncompaction; rv, right ventricle; Tnnt2, cardiac troponin T; and WT, wild-type.

aortic valve disease (0.3%; 1 in 39). Assessments of the burden of aortic valve disease in *MIB1* variant carriers were not significant (*P*>0.05).

Molecular Interactions Among CEP192, BCL7A, and NOTCH

Our results support a genetic interaction between *MIB1* and the genes identified in our LVNC family exome: *ASXL3, APCDD1, CEP192, TMX3,* and *BCL7A*. To determine if the corresponding proteins interacted in vitro, we conducted co-IP experiments in HEK293T cells. On the basis of the nature of the proteins involved, we cotransfected MIB1, N1ICD (NOTCH1 intracellular domain), or RBPJ (recombining binding protein suppressor of hairless) in pairwise combinations with the candidate interacting proteins. Thus, according to the exome data from the MIB1^{R530X} family, we cotransfected HEK293T cells with FLAG-ASXL3 plus N1ICD-myc, RBPJ-GFP, or RBP-myc expression vectors, or with APCDD1FLAG plus MIB1-HA or N1ICD-myc expression vectors. For the MIB1^{V943F} family, we cotransfected HEK293T cells with CEP192-GFP plus MIB1-HA or N1ICD-myc; with TMX3-HA plus N1ICD-myc or RBPJ-GFP; or with BCL7a-FLAG plus N1ICD-myc or RBPJ-GFP. Co-IP experiments with N1ICD or RBPJ were negative for ASXL3, APCDD1, or TMX3 (Figure S9A) but did detect interaction with CEP192 and BCL7a (Figure 5A through 5D, Figure S9B). We obtained a positive co-IP result for full-length CEP192 (192 KDa) and N1ICD (Figure S9B). To identify the region involved in this interaction, we split CEP192 in a N-terminal (amino acids [aa] 1-1322) and a C-terminal fragment (CT, aa 1323-2537). Co-IP experiments with N1ICD showed that it is the CT CEP192 region that interacts with N1ICD (Figure 5A). Thus, immunoprecipitation with anti-myc antibody and WB with anti-FLAG detected an ~150-KDa band corresponding to the CT CEP192 region. Conversely, immunoprecipitation with anti-FLAG and WB with anti-myc detected a 70-KDa band corresponding to N1ICD (Figure 5A). This region contains the T1522M mutation identified in the MIB1^{V943F} family (Figure 3B and 3D); however, the interaction with N1ICD persisted after site-directed mutagenesis to introduce the mutation into the CT fragment (Figure 5B), suggesting that the CEP192-N1ICD interaction domain may be larger. Surprisingly, co-IP did not detect interaction between CEP192 and MIB1 (Figure S9B), despite the association of MIB1 with centrosomal proteins.[79,80] In the case of BCL7A, co-IP with anti-myc antibody and WB with anti-FLAG detected a 50-KDa band corresponding to BCL7A, and the reciprocal experiment detected the 70-KDa band corresponding to N1ICD (Figure 5C). Because BCL7A is a transcription factor, we tested whether it interacted with the NOTCH effector transcription factor RBPJ cotransfecting cells with RBPJ-GFP and BCL7A-FLAG. Co-IP with anti-GFP antibody and WB with anti-FLAG detected a 50-KDa band corresponding to BCL7A, and the reciprocal experiment detected the 100-KDa band corresponding to RBPJ-GFP tagged (Figure 5D). These results support direct molecular interaction among CEP192, BCL7A, and N1ICD proteins.

DISCUSSION

Defining the genetic basis of cardiac disease has proved more challenging than anticipated, despite the technological advances in genomic analysis of the last decade.[81] The likely reason is that coding and noncoding DNA variants appear to make similar contributions to cardiac disease,[82] implying that progress toward precision cardiovascular medicine will require experimental testing of the influence of multiple potential regulatory and coding sequence variants.[83] Even in severe cardiac diseases that manifest in children or young adults (ie, congenital heart disease and cardiomyopathies) and may appear to have a single Mendelian genetic basis, phenotypic expression is influenced by multiple DNA variants, suggesting that these diseases are oligogenic[84] or polygenic.[85] This implies that the combined action of genetic modifiers can have a major effect on the expression of a cardiac disease phenotype,[3,86] making it difficult to define its genetic pathogenesis.

Our data show that mice harboring the ortholog MIB1^{R530X} and MIB1^{V943F} mutations that cause LVNC in heterozygous human carriers[34] develop LVNC when

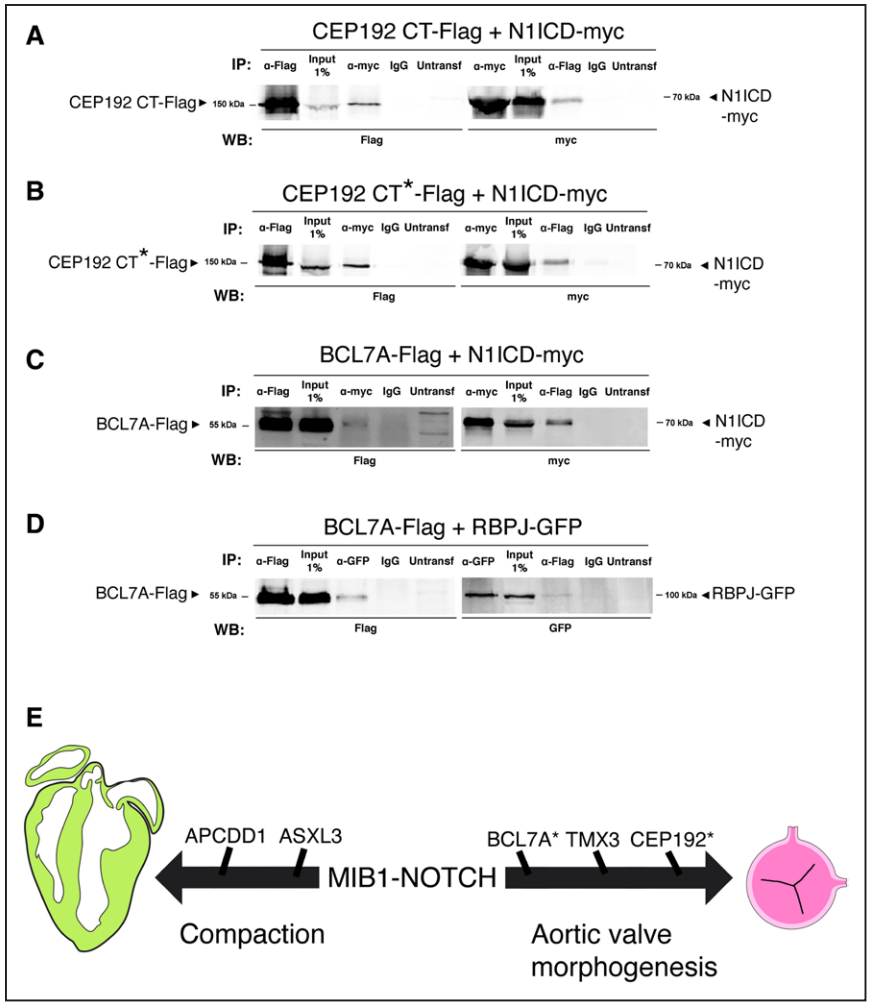

Figure 5. In vitro interaction between CEP192, BCL7A, with N1ICD or RBPJ and MIB1-NOTCH pathway interactions during compaction and aortic valve development.

A, Flag and myc immunoblotting of Flag and myc immunoprecipitates from HEK293T cells cotransfected with Flag-tagged carboxy terminal CEP192 (CEP192 CT-Flag) and myc-tagged N1ICD (N1ICD-myc). **B**, Flag and myc immunoblotting of Flag and myc immunoprecipitates from HEK293T cells cotransfected with Flag-tagged mutant carboxy terminal CEP192 (CEP192 CT*-Flag) and myc-tagged N1ICD (N1ICD-myc). **C**, Flag and myc immunoblotting of Flag and myc immunoprecipitates from HEK293T cells cotransfected with Flag-tagged BCL7A (BCL7A-Flag) and myc-tagged N1ICD (N1ICD-myc). **D**, Flag and GFP immunoblotting of Flag and GFP immunoprecipitates from HEK293T cells cotransfected with Flag-tagged BCL7A (BCL7A-Flag) and GFP-tagged RBPJ (RBPJ-GFP). **E**, Cartoon summarizing the human and mouse data. MIB1-NOTCH signaling regulates chamber compaction and aortic valve morphogenesis in humans and mice. Whole exome sequencing analysis has identified 5 candidate genes interacting with *MIB1* mutations in LVNC. Mouse modeling shows their involvement in compaction or aortic valve morphogenesis. Asterisks indicate potential biochemical interactions. CT indicates C-terminal fragment; IP, immunoprecipitation; LVNC, left ventricular noncompaction; N1ICD, NOTCH receptor 1 intracellular domain; and WB, Western blot.

cardiac MIB1 is depleted, or BAV on a MIB1 heterozygous and NOTCH-sensitized genetic background. The recessive nature of the LVNC phenotype in mice contrasts with its dominant character in humans, suggesting the existence of additional contributing genes (modifiers)[87] that interact with *MIB1* to cause LVNC in a dominant fashion in humans. Moreover, the BAV phenotype of mice heterozygous for the Mib1^{V943F} or Mib1^{R530X} mutations on a NOTCH-sensitized genetic background suggests that valve morphogenesis is strictly sensitive to the NOTCH-MIB1 dosage and that its haploinsufficiency leads to BAV. The high dosage requirement for NOTCH-MIB1 function is also supported by the observation that only 5% of mice with cardiac MIB1 depletion (Mib1$^{R530X/flox}$;Tnnt2^{CRE}) survived embryogenesis, instead of the Mendelian 12.5%. The MIB1^{V943F} mutation is deleterious in cellular assays and in zebrafish embryos,[34] and our results show that mice expressing the MIB1^{V943F} protein in the embryonic myocardium display LVNC features. In our search for additional genetic variants that contribute to LVNC, WES of families carrying the MIB1^{R530X} and MIB1^{V943F} mutations identified a set of missense variants in *ASXL3*, *APCDD1*, *CEP192*, *TMX3,* and *BCL7A* that cosegregate with the *MIB1* mutations and LVNC, suggesting a genetic interaction between *MIB1* and these modifier genes during cardiogenesis. With the exception of *BCL7A*, these genes are located on chromosome 18 close to *MIB1*, increasing the probability of cosegregation, and the exome data reveal a perfect cosegregation of these variants with *MIB1* mutations and LVNC. It remains to be determined if *MIB1* and these newly identified candidates are coordinately regulated during cardiac development.

Generation of the corresponding mouse models revealed that triple heterozygous Mib1$^{R530X/+}$ Asxl3$^{M1361V/+}$ Apcdd1$^{V150I/+}$ mice (*Thet* mice) showed features of LVNC, whereas quadruple heterozygous Mib1$^{V943F/+}$ Cep192$^{T1522M/+}$ Tmx3$^{F191X/+}$; Bcl7a$^{AG,GA/+}$ mice showed a variety of valve-related defects, including BAV. Thus, WES of our LVNC pedigrees allowed us to identify new genes contributing to LVNC or BAV. These results suggest that 2 congenital structural heart abnormalities, LVNC and BAV,[88] share a genetic substrate in which *MIB1* mutations disrupt a major developmental pathway regulating ventricular and valve development. *MIB1* mutations can thus lead to LVNC or BAV depending on their combination with a set of mutations in modifier genes that influence disease phenotype. In other words, MIB1-NOTCH signaling plays a major role in ventricular and

valve development, and its genetic disruption can lead to human LVNC or BAV in the presence of a certain genetic substrate, produced by alterations in a set of modifier genes (Figure 5E). The causal implication of *NOTCH1* mutations in BAV has been described in humans[31] and mice.[89] Likewise, *MIB1* inactivation causes LVNC in both humans and mice[34] and also BAV and valve dysmorphology in mice,[89,90] although its implication in human BAV has not been described so far.

Although patients heterozygous for the MIB1$^{V943F/+}$ CEP192$^{T1522M/+}$ TMX3$^{F191X/+}$; BCL7A$^{AG,GA/+}$ variants show LVNC and not BAV, mice carrying the 4 ortholog mutations have BAV but no LVNC, emphasizing the strong influence of the genetic background on disease phenotype and the sensitive response of inbred mouse strains (C57BL/6J) in the manifestation of cardiac phenotypes. Developmental marker analysis revealed defective chamber patterning and maturation in mice deficient for MIB1 in the myocardium, indicating the developmental origin of LVNC. Gene profiling of Mib1R530X/flox;Tnnt2Cre mice, Mib1R530X/+ Asxl3M1361V/+ Apcdd1V150I/+ triple heterozygous mice, and MIB1$^{R530X/+}$ patient-derived hiPSCs revealed shared defects in myocardial differentiation, and metabolic maturation together with increased cardiomyocyte proliferation, processes that must be tightly coordinated to achieve full cardiomyocyte maturation.[91] Mechanistically, abnormal activation of the TGFb pathway is a consistent finding across the different *Mib1* genotypes, and TGFb signaling has been related to pro-EMT and pro- or antiproliferative pathways.[92] Reinforcing this notion, persistent cardiomyocyte proliferation has been reported in mice with myocardial *Mib1* inactivation,[10,34] whereas blunted proliferation was found in a hiPSC model of LVNC with perturbed TGFb signalling.[67] Immunoprecipitation assays between NOTCH pathway elements and the proteins identified by WES suggested direct biochemical interaction of N1ICD/RBPJ with CEP192 and BCL7A. The lack of positive evidence about the other proteins may be a result of low expression or defective protein modification or folding, and thus possible interactions cannot be discarded. In addition, the genetic interaction between MIB1 and APCDD1 is worth exploring on the basis of the interplay between NOTCH and WNT in different cardiac settings.[71,93]

Previous studies have suggested the oligogenic nature of LVNC.[20,84] Our study is the first in which exome data from 2 large pedigrees reveal LVNC resulting from cosegregation of mutations in a critical gene with mutations in a set of linked modifier genes. Modeling of these mutations in mice suggests that ventricle and valve morphogenesis share, at least in part, a common genetic substrate and developmental pathway. Extrapolation of our mouse model's data to humans would imply that patients with LVNC harboring *MIB1* mutations should also be screened for valve abnormalities, and vice versa. Our study demonstrates the power of combining WES with humanized animal models generated through careful gene editing to provide mechanistic insight into complex diseases and the contribution to disease phenotype of coding and noncoding genetic variants identified through massive sequencing.

ARTICLE INFORMATION

Received December 14, 2021; accepted September 27, 2022.

Affiliations

Intercellular Signaling in Cardiovascular Development & Disease Laboratory, Centro Nacional de Investigaciones Cardiovasculares and Ciber de Enfermedades Cardiovasculares, Instituto de Salud Carlos III, Madrid, Spain (M.S.-A., A.S.-J., J.G.-B., D.M., B.P., R.P.-S., M.S., B.I., J.L.d.l.P.). Bioinformatics Unit (J.B., C.T., M.J.G., F.S.-C.), Genomics Unit (S.C., A.D.), Pluripotent Cell Technology Unit (B.P., G.G.), Translational Laboratory (B.I.), Centro Nacional de Investigaciones Cardiovasculares, Madrid, Spain. Molecular Mechanisms Program, Centro de Investigación del Cáncer and Instituto de Biología Molecular y Celular del Cáncer (Centro Nacional de Investigaciones Cardiovasculares, Universidad de Salamanca), Spain (F.S.-S., N.F.-M., A.M.P.). Laboratorio de Cardiogenética, Instituto Murciano de Investigación Biosanitaria, European Reference Networks and Unidad CSUR-European Reference Networks Guard Heart de Cardiopatias Familiares, Hospital Universitario Virgen de la Arrixaca-Universidad de Murcia, El Palmar, Spain (M.S.-M., J.R.G.-B.). Regenerative Medicine Program, Bellvitge Institute for Biomedical Research, Program for Clinical Translation of Regenerative Medicine in Catalonia, Centre for Networked Biomedical Research on Bioengineering, Biomaterials and Nanomedicine and Institució Catalana de Recerca i Estudis Avançats, Barcelona, Spain (R.E., I.R.-P., O.I.-G., A.R.). Regenerative Medicine Program, Cima Universidad de Navarra, Navarra Institute for Health Research, Pamplona, Spain (O.I.-G.). Center for Chromosome Stability and ICMM, University of Copenhagen, Denmark (M.S.). Ciber de Enfermedades Cardiovasculares, Instituto de Salud Carlos III, Madrid, Spain (S.C., A.D.). MRC London Institute of Medical Sciences (D.O., K.A.M.), National Heart and Lung Institute (K.A.M.), Imperial College London, United Kingdom. Cardiology Department, IIS-Fundación Jiménez Díaz Hospital, Madrid, Spain (B.I.). Instituto de Investigación Biomédica de A Coruña and Departamento Científico, Health in Code S.L., A Coruña, Spain (L.M.). Department of Animal Biology, Faculty of Sciences, Instituto de Investigación Biomédica de Málaga and BIONAND, Centro Andaluz de Nanomedicina y Biotecnología, Universidad de Málaga, Spain (J.P.-P.).

Acknowledgments

The authors thank the Centro Nacional de Investigaciones Cardiovasculares Transgenesis and Microscopy Units for technical support. They thank A. Galicia and L. Méndez for mouse husbandry, and S. Bartlett for English editing. This research has been conducted using the United Kingdom Biobank Resource under application no. 40616.

Sources of Funding

This study was supported by grants PID2019-104776RB-I00 and PID2020-120326RB-I00, CB16/11/00399 (CIBER CV) financed by MCIN/AEI/10.13039/501100011033, a grant from the Fundación BBVA (Ref. BIO14_298), and a grant from Fundació La Marató de TV3 (Ref. 20153431) to J.L.d.l.P. M.S.-A. was supported by a PhD contract from the Severo Ochoa Predoctoral Program (SVP-2014-068723) of the MCIN/AEI/10.13039/501100011033. J.R.G.-B. was supported by SEC/FEC-INV-BAS 21/021. A.R. was funded by grants from MCIN (PID2021123925OB-I00), TerCel (RD16/0011/0024), AGAUR (2017-SGR-899), and Fundació La Marató de TV3 (201534-30). J.M.P.-P. was supported by RTI2018-095410-B-I00 (MCIN) and PY2000443 (Junta de Andalucía). B.I. was supported by the European Commission (H2020-HEALTH grant No. 945118) and by MCIN (PID2019-107332RB-I00). DO'R was supported by the Medical Research Council (MC-A658-5QEB0) and KAMcG by the British Heart Foundation (RG/19/6/34387, RE/18/4/34215). The cost of this publication was supported in part with funds from the European Regional Development Fund. The Centro Nacional de Investigaciones Cardiovasculares is supported by the ISCIII, the MCIN, and the Pro Centro Nacional de Investigaciones Cardiovasculares Foundation and is a Severo Ochoa Center of Excellence (grant CEX2020001041-S) financed by MCIN/AEI/10.13039/501100011033. For the purpose of open access, the authors have applied a CC BY public copyright license to any Author Accepted Manuscript version arising.

Disclosures

None.

Supplemental Material

Supplemental Methods
Figures S1–S9
Tables S1–S12
References 94–112

REFERENCES

1. Bos JM, Towbin JA, Ackerman MJ. Diagnostic, prognostic, and therapeutic implications of genetic testing for hypertrophic cardiomyopathy. *J Am Coll Cardiol.* 2009;54:201201211–201201211. doi: 10.1016/j.jacc.2009.02.075
2. Watkins H, Ashrafian H, Redwood C. Inherited cardiomyopathies. *N Engl J Med.* 2011;364:1643–1656. doi: 10.1056/NEJMra0902923
3. Puckelwartz MJ, Pesce LL, Dellefave-Castillo LM, Wheeler MT, Pottinger TD, Robinson AC, Kearns SD, Gacita AM, Schoppen ZJ, Pan W, et al. Genomic context differs between human dilated cardiomyopathy and hypertrophic cardiomyopathy. *J Am Heart Assoc.* 2021;10:e019944. doi: 10.1161/JAHA.120.019944
4. Ritter M, Oechslin E, Sutsch G, Attenhofer C, Schneider J, Jenni R. Isolated noncompaction of the myocardium in adults. *Mayo Clin Proc.* 1997;72:26–31. doi: 10.4065/72.1.26
5. Chin TK, Perloff JK, Williams RG, Jue K, Mohrmann R. Isolated noncompaction of left ventricular myocardium. A study of eight cases. *Circulation.* 1990;82:507–513. doi: 10.1161/01.cir.82.2.507
6. Jenni R, Oechslin EN, van der Loo B. Isolated ventricular non-compaction of the myocardium in adults. *Heart.* 2007;93:11–15. doi: 10.1136/hrt.2005.082271
7. Sedmera D, Pexieder T, Vuillemin M, Thompson RP, Anderson RH. Developmental patterning of the myocardium. *Anat Rec.* 2000;258:319–337. doi: 10.1002/(SICI)1097-0185(20000401)258:4<319::AID-AR1>3.0.CO;2-O
8. Tian X, Li Y, He L, Zhang H, Huang X, Liu Q, Pu W, Zhang L, Li Y, Zhao H, et al. Identification of a hybrid myocardial zone in the mammalian heart after birth. *Nat Commun.* 2017;8:87. doi: 10.1038/s41467-017-00118-1
9. Faber JW, D'Silva A, Christoffels VM, Jensen B. Lack of morphometric evidence for ventricular compaction in humans. *J Cardiol.* 2021; doi: 10.1016/j.jjcc.2021.03.006
10. D'Amato G, Luxan G, del Monte-Nieto G, Martinez-Poveda B, Torroja C, Walter W, Bochter MS, Benedito R, Cole S, Martinez F, et al. Sequential Notch activation regulates ventricular chamber development. *Nat Cell Biol.* 2016;18:7–20. doi: 10.1038/ncb3280
11. Freedom RM, Yoo SJ, Perrin D, Taylor G, Petersen S, Anderson RH. The morphological spectrum of ventricular noncompaction. *Cardiol Young.* 2005;15:345–364. doi: 10.1017/S1047951105000752
12. Nucifora G, Aquaro GD, Pingitore A, Masci PG, Lombardi M. Myocardial fibrosis in isolated left ventricular non-compaction and its relation to disease severity. *Eur J Heart Fail.* 2011;13:170–176. doi: 10.1093/eurjhf/hfq222
13. Jenni R, Oechslin E, Schneider J, Attenhofer Jost C, Kaufmann PA. Echocardiographic and pathoanatomical characteristics of isolated left ventricular non-compaction: a step towards classification as a distinct cardiomyopathy. *Heart.* 2001;86:666–671. doi: 10.1136/heart.86.6.666
14. Oechslin EN, Attenhofer Jost CH, Rojas JR, Kaufmann PA, Jenni R. Long-term follow-up of 34 adults with isolated left ventricular noncompaction: a distinct cardiomyopathy with poor prognosis. *J Am Coll Cardiol.* 2000;36:493–500. doi: 10.1016/s0735-1097(00)00755-5
15. Captur G, Nihoyannopoulos P. Left ventricular non-compaction: genetic heterogeneity, diagnosis and clinical course. *Int J Cardiol.* 2010;140:145–153. doi: 10.1016/j.ijcard.2009.07.003
16. Ichida F. Left ventricular noncompaction. *Circ J.* 2009;73:19–26. doi: 10.1253/circj.cj-08-0995
17. Towbin JA, Lorts A, Jefferies JL. Left ventricular non-compaction cardiomyopathy. *Lancet.* 2015;386:813–825. doi: 10.1016/S0140-6736(14)61282-4
18. Hoedemaekers YM, Caliskan K, Michels M, Frohn-Mulder I, van der Smagt JJ, Phefferkorn JE, Wessels MW, ten Cate FJ, Sijbrands EJ, Dooijes D, et al. The importance of genetic counseling, DNA diagnostics, and cardiologic family screening in left ventricular noncompaction cardiomyopathy. *Circ Cardiovasc Genet.* 2010;3:232–239. doi: 10.1161/CIRCGENETICS.109.903898
19. Klaassen S, Probst S, Oechslin E, Gerull B, Krings G, Schuler P, Greutmann M, Hurlimann D, Yegitbasi M, Pons L, et al. Mutations in sarcomere protein genes in left ventricular noncompaction. *Circulation.* 2008;117:2893–2901. doi: 10.1161/CIRCULATIONAHA.107.746164
20. van Waning JI, Caliskan K, Hoedemaekers YM, van Spaendonck-Zwarts KY, Baas AF, Boekholdt SM, van Melle JP, Teske AJ, Asselbergs FW, Backx A, et al. Genetics, clinical features, and long-term outcome of noncompaction cardiomyopathy. *J Am Coll Cardiol.* 2018;71:711–722. doi: 10.1016/j.jacc.2017.12.019
21. Ichida F, Tsubata S, Bowles KR, Haneda N, Uese K, Miyawaki T, Dreyer WJ, Messina J, Li H, Bowles NE, et al. Novel gene mutations in patients with left ventricular noncompaction or Barth syndrome. *Circulation.* 2001;103:1256–1263. doi: 10.1161/01.cir.103.9.1256
22. Sedaghat-Hamedani F, Haas J, Zhu F, Geier C, Kayvanpour E, Liss M, Lai A, Frese K, PribeWolferts R, Amr A, et al. Clinical genetics and outcome of left ventricular noncompaction cardiomyopathy. *Eur Heart J.* 2017;38:3449–3460. doi: 10.1093/eurheartj/ehx545
23. Grego-Bessa J, Luna-Zurita L, del Monte G, Bolos V, Melgar P, Arandilla A, Garratt AN, Zang H, Mukouyama YS, Chen H, et al. Notch signaling is essential for ventricular chamber development. *Dev Cell.* 2007;12:415–429. doi: 10.1016/j.devcel.2006.12.011
24. Zhang W, Chen H, Qu X, Chang CP, Shou W. Molecular mechanism of ventricular trabeculation/compaction and the pathogenesis of the left ventricular noncompaction cardiomyopathy (LVNC). *Am J Med Genet C Semin Med Genet.* 2013;163C:144–156. doi: 10.1002/ajmg.c.31369
25. Choquet C, Nguyen THM, Sicard P, Buttigieg E, Tran TT, Kober F, Varlet I, Sturny R, Costa MW, Harvey RP, et al. Deletion of Nkx2-5 in trabecular myocardium reveals the developmental origins of pathological heterogeneity associated with ventricular noncompaction cardiomyopathy. *PLoS Genet.* 2018;14:e1007502. doi: 10.1371/journal.pgen.1007502
26. Artavanis-Tsakonas S, Rand MD, Lake RJ. Notch signaling: cell fate control and signal integration in development. *Science.* 1999;284:770–776. doi: 10.1126/science.284.5415.770
27. Kopan R. Notch signaling. *Cold Spring Harb Perspect Biol.* 2012;4: doi: 10.1101/cshperspect.a011213
28. Joutel A, Corpechot C, Ducros A, Vahedi K, Chabriat H, Mouton P, Alamowitch S, Domenga V, Cecillion M, Marechal E, et al. Notch3 mutations in CADASIL, a hereditary adult-onset condition causing stroke and dementia. *Nature.* 1996;383:707–710. doi: 10.1038/383707a0
29. Li L, Krantz ID, Deng Y, Genin A, Banta AB, Collins CC, Qi M, Trask BJ, Kuo WL, Cochran J, et al. Alagille syndrome is caused by mutations in human Jagged1, which encodes a ligand for Notch1. *Nat Genet.* 1997;16:243–251. doi: 10.1038/ng0797-243
30. Oda T, Elkahloun AG, Pike BL, Okajima K, Krantz ID, Genin A, Piccoli DA, Meltzer PS, Spinner NB, Collins FS, et al. Mutations in the human Jagged1 gene are responsible for Alagille syndrome. *Nat Genet.* 1997;16:235–242. doi: 10.1038/ng0797-235
31. Garg V, Muth AN, Ransom JF, Schluterman MK, Barnes R, King IN, Grossfeld PD, Srivastava D. Mutations in NOTCH1 cause aortic valve disease. *Nature.* 2005;437:270274.
32. MacGrogan D, Munch J, de la Pompa JL. Notch and interacting signalling pathways in cardiac development, disease, and regeneration. *Nat Rev Cardiol.* 2018;15:685–704. doi: 10.1038/s41569-018-0100-2
33. Meester JAN, Verstraeten A, Alaerts M, Schepers D, Van Laer L, Loeys BL. Overlapping but distinct roles for NOTCH receptors in human cardiovascular disease. *Clin Genet.* 2019;95:85–94. doi: 10.1111/cge.13382
34. Luxan G, Casanova JC, Martinez-Poveda B, Prados B, D'Amato G, MacGrogan D, Gonzalez-Rajal A, Dobarro D, Torroja C, Martinez F, et al. Mutations in the NOTCH pathway regulator MIB1 cause left ventricular noncompaction cardiomyopathy. *Nat Med.* 2013;19:193–201. doi: 10.1038/nm.3046
35. Itoh M, Kim CH, Palardy G, Oda T, Jiang YJ, Maust D, Yeo SY, Lorick K, Wright GJ, ArizaMcNaughton L, et al. Mind bomb is a ubiquitin ligase that is essential for efficient activation of Notch signaling by Delta. *Dev Cell.* 2003;4:67–82. doi: 10.1016/s1534-5807(02)00409-4
36. Jiao K, Kulessa H, Tompkins K, Zhou Y, Batts L, Baldwin HS, Hogan BL. An essential role of Bmp4 in the atrioventricular septation of the mouse heart. *Genes Dev.* 2003;17:2362–2367. doi: 10.1101/gad.1124803
37. Agah R, Frenkel PA, French BA, Michael LH, Overbeek PA, Schneider MD. Gene recombination in postmitotic cells. Targeted expression of Cre recombinase provokes cardiac-restricted, site-specific rearrangement in adult ventricular muscle in vivo. *J Clin Invest.* 1997;100:169–179. doi: 10.1172/JCI119509

38. Stanley EG, Biben C, Elefanty A, Barnett L, Koentgen F, Robb L, Harvey RP. Efficient Cre-mediated deletion in cardiac progenitor cells conferred by a 3'UTR-ires-Cre allele of the homeobox gene Nkx2-5. *Int J Dev Biol.* 2002;46:431–439.
39. Koo BK, Yoon MJ, Yoon KJ, Im SK, Kim YY, Kim CH, Suh PG, Jan YN, Kong YY. An obligatory role of mind bomb-1 in notch signaling of mammalian development. *PLoS One.* 2007;2:e1221. doi: 10.1371/journal.pone.0001221
40. Conlon RA, Reaume AG, Rossant J. Notch1 is required for the coordinate segmentation of somites. *Development.* 1995;121:1533–1545. doi: 10.1242/dev.121.5.1533
41. Oliveros JC, Franch M, Tabas-Madrid D, San-Leon D, Montoliu L, Cubas P, Pazos F. Breaking-Cas-interactive design of guide RNAs for CRISPR-Cas experiments for ENSEMBLgenomes. *Nucleic Acids Res.* 2016;44:W267–W271. doi: 10.1093/nar/gkw407
42. Concordet JP, Haeussler M. CRISPOR: intuitive guide selection for CRISPR/Cas9 genome editing experiments and screens. *Nucleic Acids Res.* 2018;46:W242–W245. doi: 10.1093/nar/gky354
43. Cong L, Ran FA, Cox D, Lin S, Barretto R, Habib N, Hsu PD, Wu X, Jiang W, Marraffini LA, et al. Multiplex genome engineering using CRISPR/Cas systems. *Science.* 2013;339:819–823. doi: 10.1126/science.1231143
44. Harms DW, Quadros RM, Seruggia D, Ohtsuka M, Takahashi G, Montoliu L, Gurumurthy CB. Mouse genome editing using the CRISPR/Cas system. *Curr Protoc Hum Genet.* 2014;83:15 17 11--15 17 127. doi: 10.1002/0471142905.hg1507s83
45. Richardson CD, Ray GJ, Bray NL, Corn JE. Non-homologous DNA increases gene disruption efficiency by altering DNA repair outcomes. *Nat Commun.* 2016;7:12463. doi: 10.1038/ncomms12463
46. Stollberger C, Finsterer J. Left ventricular hypertrabeculation/noncompaction. *J Am Soc Echocardiogr.* 2004;17:91–100. doi: 10.1016/S0894-7317(03)00514-5
47. Stollberger C, Finsterer J, Blazek G. Left ventricular hypertrabeculation/noncompaction and association with additional cardiac abnormalities and neuromuscular disorders. *Am J Cardiol.* 2002;90:899–902. doi: 10.1016/s0002-9149(02)02723-6
48. DePristo MA, Banks E, Poplin R, Garimella KV, Maguire JR, Hartl C, Philippakis AA, del Angel G, Rivas MA, Hanna M, et al. A framework for variation discovery and genotyping using next-generation DNA sequencing data. *Nat Genet.* 2011;43:491–498. doi: 10.1038/ng.806
49. Bolger AM, Lohse M, Usadel B. Trimmomatic: a flexible trimmer for Illumina sequence data. *Bioinformatics.* 2014;30:2114–2120. doi: 10.1093/bioinformatics/btu170
50. Li H, Durbin R. Fast and accurate short read alignment with Burrows-Wheeler transform. *Bioinformatics.* 2009;25:1754–1760. doi: 10.1093/bioinformatics/btp324
51. McLaren W, Gil L, Hunt SE, Riat HS, Ritchie GR, Thormann A, Flicek P, Cunningham F. The Ensembl variant effect predictor. *Genome Biol.* 2016;17:122. doi: 10.1186/s13059016-0974-4
52. McKenna A, Hanna M, Banks E, Sivachenko A, Cibulskis K, Kernytsky A, Garimella K, Altshuler D, Gabriel S, Daly M, et al. The Genome Analysis Toolkit: a MapReduce framework for analyzing next-generation DNA sequencing data. *Genome Res.* 2010;20:1297–1303. doi: 10.1101/gr.107524.110
53. Van der Auwera GA, Carneiro MO, Hartl C, Poplin R, Del Angel , G, Levy-Moonshine A, Jordan T, Shakir K, Roazen D, et al. From FastQ data to high confidence variant calls: the Genome Analysis Toolkit best practices pipeline. *Curr Protoc Bioinformatics.* 2013;43:11 10 11--111 10 33. doi: 10.1002/0471250953.bi1110s43
54. Landrum MJ, Lee JM, Riley GR, Jang W, Rubinstein WS, Church DM, Maglott DR. ClinVar: public archive of relationships among sequence variation and human phenotype. *Nucleic Acids Res.* 2014;42:D980–D985. doi: 10.1093/nar/gkt1113
55. Karczewski KJ, Francioli LC, Tiao G, Cummings BB, Alfoldi J, Wang Q, Collins RL, Laricchia KM, Ganna A, Birnbaum DP, et al; Genome Aggregation Database Consortium. The mutational constraint spectrum quantified from variation in 141,456 humans. *Nature.* 2020;581:434–443. doi: 10.1038/s41586-020-2308-7
56. Kircher M, Witten DM, Jain P, O'Roak BJ, Cooper GM, Shendure J. A general framework for estimating the relative pathogenicity of human genetic variants. *Nat Genet.* 2014;46:310–315. doi: 10.1038/ng.2892
57. Adzhubei IA, Schmidt S, Peshkin L, Ramensky VE, Gerasimova A, Bork P, Kondrashov AS, Sunyaev SR. A method and server for predicting damaging missense mutations. *Nat Methods.* 2010;7:248–249. doi: 10.1038/nmeth0410-248
58. Davydov EV, Goode DL, Sirota M, Cooper GM, Sidow A, Batzoglou S. Identifying a high fraction of the human genome to be under selective constraint using GERP++. *PLoS Comput Biol.* 2010;6:e1001025. doi: 10.1371/journal.pcbi.1001025
59. Walsh R, Thomson KL, Ware JS, Funke BH, Woodley J, McGuire KJ, Mazzarotto F, Blair E, Seller A, Taylor JC, et al. Reassessment of Mendelian gene pathogenicity using 7,855 cardiomyopathy cases and 60,706 reference samples. *Genet Med.* 2017;19:192–203. doi: 10.1038/gim.2016.90
60. Huntley RP, Sawford T, Mutowo-Meullenet P, Shypitsyna A, Bonilla C, Martin MJ, O'Donovan C. The GOA database: gene ontology annotation updates for 2015. *Nucleic Acids Res.* 2015;43:D1057–D1063. doi: 10.1093/nar/gku1113
61. Barrett T, Wilhite SE, Ledoux P, Evangelista C, Kim IF, Tomashevsky M, Marshall KA, Phillippy KH, Sherman PM, Holko M, et al. NCBI GEO: archive for functional genomics data sets--update. *Nucleic Acids Res.* 2013;41:D991–D995. doi: 10.1093/nar/gks1193
62. Diez-Roux G, Banfi S, Sultan M, Geffers L, Anand S, Rozado D, Magen A, Canidio E, Pagani M, Peluso I, et al. A high-resolution anatomical atlas of the transcriptome in the mouse embryo. *PLoS Biol.* 2011;9:e1000582. doi: 10.1371/journal.pbio.1000582
63. Wang X, Xin Q, Li L, Li J, Zhang C, Qiu R, Qian C, Zhao H, Liu Y, Shan S, et al. Exome sequencing reveals a heterozygous DLX5 mutation in a Chinese family with autosomal dominant split-hand/foot malformation. *Eur J Hum Genet.* 2014;22:110511051110–110511051110. doi: 10.1038/ejhg.2014.7
64. Li J, Miao L, Shieh D, Spiotto E, Li J, Zhou B, Paul A, Schwartz RJ, Firulli AB, Singer HA, et al. Single-cell lineage tracing reveals that oriented cell division contributes to trabecular morphogenesis and regional specification. *Cell Rep.* 2016;15:158–170. doi: 10.1016/j.celrep.2016.03.012
65. Meilhac SM, Esner M, Kerszberg M, Moss JE, Buckingham ME. Oriented clonal cell growth in the developing mouse myocardium underlies cardiac morphogenesis. *J Cell Biol.* 2004;164:97–109. doi: 10.1083/jcb.200309160
66. Lian X, Zhang J, Azarin SM, Zhu K, Hazeltine LB, Bao X, Hsiao C, Kamp TJ, Palecek SP. Directed cardiomyocyte differentiation from human pluripotent stem cells by modulating Wnt/beta-catenin signaling under fully defined conditions. *Nat Protoc.* 2013;8:162–175. doi: 10.1038/nprot.2012.150
67. Kodo K, Ong SG, Jahanbani F, Termglinchan V, Hirono K, InanlooRahatloo K, Ebert AD, Shukla P, Abilez OJ, Churko JM, et al. iPSC-derived cardiomyocytes reveal abnormal TGF-beta signalling in left ventricular noncompaction cardiomyopathy. *Nat Cell Biol.* 2016;18:1031–1042. doi: 10.1038/ncb3411
68. D'Amato G, Luxan G, de la Pompa JL. Notch signalling in ventricular chamber development & cardiomyopathy. *FEBS J.* 2016; doi: 10.1111/febs.13773
69. Bergmann O, Bhardwaj RD, Bernard S, Zdunek S, Barnabe-Heider F, Walsh S, Zupicich J, Alkass K, Buchholz BA, Druid H, et al. Evidence for cardiomyocyte renewal in humans. *Science.* 2009;324:98–102. doi: 10.1126/science.1164680
70. Shimomura Y, Agalliu D, Vonica A, Luria V, Wajid M, Baumer A, Belli S, Petukhova L, Schinzel A, Brivanlou AH, et al. APCDD1 is a novel Wnt inhibitor mutated in hereditary hypotrichosis simplex. *Nature.* 2010;464:1043–1047. doi: 10.1038/nature08875
71. Wang Y, Wu B, Chamberlain AA, Lui W, Koirala P, Susztak K, Klein D, Taylor V, Zhou B. Endocardial to myocardial notch-wnt-bmp axis regulates early heart valve development. *PLoS One.* 2013;8:e60244. doi: 10.1371/journal.pone.0060244
72. Fu F, Li R, Lei TY, Wang D, Yang X, Han J, Pan M, Zhen L, Li J, Li FT, et al. Compound heterozygous mutation of the ASXL3 gene causes autosomal recessive congenital heart disease. *Hum Genet.* 2021;140:333–348. doi: 10.1007/s00439-020-02200-z
73. Gomez-Ferreria MA, Rath U, Buster DW, Chanda SK, Caldwell JS, Rines DR, Sharp DJ. Human Cep192 is required for mitotic centrosome and spindle assembly. *Curr Biol.* 2007;17:1960–1966. doi: 10.1016/j.cub.2007.10.019
74. Haugstetter J, Maurer MA, Blicher T, Pagac M, Wider G, Ellgaard L. Structure-function analysis of the endoplasmic reticulum oxidoreductase TMX3 reveals interdomain stabilization of the N-terminal redox-active domain. *J Biol Chem.* 2007;282:338593385933867–338593385933867. doi: 10.1074/jbc.m706442200
75. Chao R, Nevin L, Agarwal P, Riemer J, Bai X, Delaney A, Akana M, JimenezLopez N, Bardakjian T, Schneider A, et al. A male with unilateral microphthalmia reveals a role for TMX3 in eye development. *PLoS One.* 2010;5:e10565. doi: 10.1371/journal.pone.0010565
76. Balinas-Gavira C, Rodriguez MI, Andrades A, Cuadros M, Alvarez-Perez JC, AlvarezPrado AF, de Yebenes VG, Sanchez-Hernandez S, Fernandez-Vigo E, Munoz J, et al. Frequent mutations in the amino-terminal domain of BCL7A impair its tumor suppressor role in DLBCL. *Leukemia.* 2020;34:2722–2735. doi: 10.1038/s41375-020-0919-5

77. Fairley S, Lowy-Gallego E, Perry E, Flicek P. The International Genome Sample Resource (IGSR) collection of open human genomic variation resources. *Nucleic Acids Res.* 2020;48:D941–D947. doi: 10.1093/nar/gkz836
78. Reddy YNV, Melenovsky V, Redfield MM, Nishimura RA, Borlaug BA. High-output heart failure: a 15-year experience. *J Am Coll Cardiol.* 2016; 68:473–482. doi: 10.1016/j.jacc.2016.05.043
79. Tozer S, Baek C, Fischer E, Goiame R, Morin X. Differential routing of Mindbomb1 via centriolar satellites regulates asymmetric divisions of neural progenitors. *Neuron.* 2017;93:542–551.e4. doi: 10.1016/j.neuron.2016.12.042
80. Villumsen BH, Danielsen JR, Povlsen L, Sylvestersen KB, Merdes A, Beli P, Yang YG, Choudhary C, Nielsen ML, Mailand N, et al. A new cellular stress response that triggers centriolar satellite reorganization and ciliogenesis. *EMBO J.* 2013;32:3029–3040. doi: 10.1038/emboj.2013.223
81. Morton SU, Quiat D, Seidman JG, Seidman CE. Genomic frontiers in congenital heart disease. *Nat Rev Cardiol.* 2021; doi: 10.1038/s41569-021-00587-4
82. Richter F, Morton SU, Kim SW, Kitaygorodsky A, Wasson LK, Chen KM, Zhou J, Qi H, Patel N, DePalma SR, et al. Genomic analyses implicate noncoding de novo variants in congenital heart disease. *Nat Genet.* 2020;52:769–777. doi: 10.1038/s41588-020-0652-z
83. Dainis AM, Ashley EA. Cardiovascular precision medicine in the genomics era. *JACC Basic Transl Sci.* 2018;3:313–326. doi: 10.1016/j.jacbts.2018.01.003
84. Gifford CA, Ranade SS, Samarakoon R, Salunga HT, de Soysa TY, Huang Y, Zhou P, Elfenbein A, Wyman SK, Bui YK, et al. Oligogenic inheritance of a human heart disease involving a genetic modifier. *Science.* 2019; 364:865–870. doi: 10.1126/science.aat5056
85. Tadros R, Francis C, Xu X, Vermeer AMC, Harper AR, Huurman R, Kelu Bisabu K, Walsh R, Hoorntje ET, Te Rijdt WP, et al. Shared genetic pathways contribute to risk of hypertrophic and dilated cardiomyopathies with opposite directions of effect. *Nat Genet.* 2021;53:128–134. doi: 10.1038/s41588-020-00762-2
86. Harper AR, Goel A, Grace C, Thomson KL, Petersen SE, Xu X, Waring A, Ormondroyd E, Kramer CM, Ho CY, et al; HCMR Investigators. Common genetic variants and modifiable risk factors underpin hypertrophic cardiomyopathy susceptibility and expressivity. *Nat Genet.* 2021;53:135–142. doi: 10.1038/s41588-020-00764-0
87. Kousi M, Katsanis N. Genetic modifiers and oligogenic inheritance. *Cold Spring Harb Perspect Med.* 2015;5: doi: 10.1101/cshperspect.a017145
88. Curfman G. Bicuspid aortic valve-a common form of structural heart disease. *JAMA.* 2021;325:540–541. doi: 10.1001/jama.2021.0109
89. MacGrogan D, D'Amato G, Travisano S, Martinez-Poveda B, Luxan G, Del Monte-Nieto G, Papoutsi T, Sbroggio M, Bou V, Gomez-Del Arco P, et al. Sequential ligand-dependent Notch signaling activation regulates valve primordium formation and morphogenesis. *Circ Res.* 2016;118:1480–1497. doi: 10.1161/CIRCRESAHA.115.308077
90. Captur G, Wilson R, Bennett MF, Luxan G, Nasis A, de la Pompa JL, Moon JC, Mohun TJ. Morphogenesis of myocardial trabeculae in the mouse embryo. *J Anat.* 2016;229:314325. doi: 10.1111/joa.12465
91. Guo Y, Pu WT. Cardiomyocyte maturation: new phase in development. *Circ Res.* 2020;126:1086–1106. doi: 10.1161/CIRCRESAHA.119.315862
92. Zhang Y, Alexander PB, Wang XF. TGF-beta family signaling in the control of cell proliferation and survival. *Cold Spring Harb Perspect Biol.* 2017;9: doi: 10.1101/cshperspect.a022145
93. Zhao L, Ben-Yair R, Burns CE, Burns CG. Endocardial Notch signaling promotes cardiomyocyte proliferation in the regenerating zebrafish heart through Wnt pathway antagonism. *Cell Rep.* 2019;26:546–554.e5. doi: 10.1016/j.celrep.2018.12.048
94. Raya A, Rodriguez-Piza I, Guenechea G, Vassena R, Navarro S, Barrero MJ, Consiglio A, Castella M, Rio P, Sleep E, et al. Disease-corrected haematopoietic progenitors from Fanconi anaemia induced pluripotent stem cells. *Nature.* 2009;460:53–59. doi: 10.1038/nature08129
95. Sanchez-Danes A, Richaud-Patin Y, Carballo-Carbajal I, Jimenez-Delgado S, Caig C, Mora S, Di Guglielmo C, Ezquerra M, Patel B, Giralt A, et al. Disease-specific phenotypes in dopamine neurons from human iPS-based models of genetic and sporadic Parkinson's disease. *EMBO Mol Med.* 2012;4:380–395. doi: 10.1002/emmm.201200215
96. Ran FA, Hsu PD, Wright J, Agarwala V, Scott DA, Zhang F. Genome engineering using the CRISPR-Cas9 system. *Nat Protoc.* 2013;8:2281–2308. doi: 10.1038/nprot.2013.143
97. Calatayud C, Carola G, Fernandez-Carasa I, Valtorta M, Jimenez-Delgado S, Diaz M, Soriano-Fradera J, Cappelletti G, Garcia-Sancho J, Raya A, et al. CRISPR/Cas9-mediated generation of a tyrosine hydroxylase reporter iPSC line for live imaging and isolation of dopaminergic neurons. *Sci Rep.* 2019;9:6811. doi: 10.1038/s41598-019-43080-2
98. Valls-Margarit M, Iglesias-Garcia O, Di Guglielmo C, Sarlabous L, Tadevosyan K, Paoli R, Comelles J, Blanco-Almazan D, Jimenez-Delgado S, Castillo-Fernandez O, et al. Engineered macroscale cardiac constructs elicit human myocardial tissue-like functionality. *Stem Cell Rep.* 2019;13:207–220. doi: 10.1016/j.stemcr.2019.05.024
99. Kanzler B, Kuschert SJ, Liu YH, Mallo M. Hoxa-2 restricts the chondrogenic domain and inhibits bone formation during development of the branchial area. *Development.* 1998;125:2587–2597. doi: 10.1242/dev.125.14.2587
100. Yang J, Bucker S, Jungblut B, Bottger T, Cinnamon Y, Tchorz J, Muller M, Bettler B, Harvey R, Sun QY, et al. Inhibition of Notch2 by Numb/Numblike controls myocardial compaction in the heart. *Cardiovasc Res.* 2012;96:276–285. doi: 10.1093/cvr/cvs250
101. Chen H, Zhang W, Li D, Cordes TM, Mark Payne R, Shou W. Analysis of ventricular hypertrabeculation and noncompaction using genetically engineered mouse models. *Pediatr Cardiol.* 2009;30:626–634. doi: 10.1007/s00246-009-9406-5
102. Martin M. CUTADAPT removes adapter sequences from high-throughput sequencing reads. *EMBnetjournal.* 2011;17:10–12. doi: 10.14806/ej.17.1.200
103. Li B, Dewey CN. RSEM: accurate transcript quantification from RNA-seq data with or without a reference genome. *BMC Bioinf.* 2011;12:323. doi: 10.1186/1471-2105-12-323
104. Robinson MD, McCarthy DJ, Smyth GK. edgeR: a Bioconductor package for differential expression analysis of digital gene expression data. *Bioinformatics.* 2010;26:139–140. doi: 10.1093/bioinformatics/btp616
105. Kramer A, Green J, Pollard J Jr, Tugendreich S. Causal analysis approaches in Ingenuity Pathway Analysis. *Bioinformatics.* 2014;30:523–530. doi: 10.1093/bioinformatics/btt703
106. Subramanian A, Tamayo P, Mootha VK, Mukherjee S, Ebert BL, Gillette MA, Paulovich A, Pomeroy SL, Golub TR, Lander ES, et al. Gene set enrichment analysis: a knowledge-based approach for interpreting genome-wide expression profiles. *Proc Natl Acad Sci USA.* 2005;102:15545–15550. doi: 10.1073/pnas.0506580102
107. Cruz-Adalia A, Jimenez-Borreguero LJ, Ramirez-Huesca M, Chico-Calero I, Barreiro O, Lopez-Conesa E, Fresno M, Sanchez-Madrid F, Martin P. CD69 limits the severity of cardiomyopathy after autoimmune myocarditis. *Circulation.* 2010;122:1396–1404. doi: 10.1161/circulationaha.110.952820
108. van de Weijer T, van Ewijk PA, Zandbergen HR, Slenter JM, Kessels AG, Wildberger JE, Hesselink MK, Schrauwen P, Schrauwen-Hinderling VB, Kooi ME. Geometrical models for cardiac MRI in rodents: comparison of quantification of left ventricular volumes and function by various geometrical models with a full-volume MRI data set in rodents. *Am J Physiol Heart Circ Physiol.* 2012;302:H709–H715. doi: 10.1152/ajpheart.00710.2011
109. Sudlow C, Gallacher J, Allen N, Beral V, Burton P, Danesh J, Downey P, Elliott P, Green J, Landray M, et al. UK Biobank: an open access resource for identifying the causes of a wide range of complex diseases of middle and old age. *PLoS Med.* 2015;12:e1001779. doi: 10.1371/journal.pmed.1001779
110. Backman JD, Li AH, Marcketta A, Sun D, Mbatchou J, Kessler MD, Benner C, Liu D, Locke AE, Balasubramanian S, et al; Regeneron Genetics Center. Exome sequencing and analysis of 454,787 UK Biobank participants. *Nature.* 2021;599:628–634. doi: 10.1038/s41586-021-04103-z
111. McLaren W, Pritchard B, Rios D, Chen Y, Flicek P, Cunningham F. Deriving the consequences of genomic variants with the Ensembl API and SNP Effect Predictor. *Bioinformatics.* 2010;26:2069–2070. doi: 10.1093/bioinformatics/btq330
112. Jaganathan K, Kyriazopoulou Panagiotopoulou S, McRae JF, Darbandi SF, Knowles D, Li YI, Kosmicki JA, Arbelaez J, Cui W, Schwartz GB, et al. Predicting Splicing from Primary Sequence with Deep Learning. *Cell.* 2019;176:535–548.e24. doi: 10.1016/j.cell.2018.12.015